JOURNAL OF GEOPHYSICAL RESEARCH, VOL. 91, NO. A4, PAGES 4491–4512, APRIL 1, 1986

Simultaneous H_α Line Profile and Radar Measurements at Arecibo

R. B. KERR AND S. K. ATREYA

Department of Atmospheric and Oceanic Science, University of Michigan, Ann Arbor

J. W. MERIWETHER, JR.

Space Physics Research Laboratory, University of Michigan, Ann Arbor

C. A. TEPLEY, AND R. G. BURNSIDE

Arecibo Observatory, Arecibo, Puerto Rico

High resolution measurements of the geocoronal Balmer alpha (H_α) emission were made with a Fabry-Perot interferometer at Arecibo, Puerto Rico, in six observing campaigns between March 1980 and November 1984. Four of these included simultaneous radar measurements of the topside F region. The nighttime variation of the zenith H_α intensity is highly symmetric about solar midnight. However, effective hydrogen temperatures near the morning exobase are generally hotter than near the evening exobase, implying a depletion of exobase hydrogen density in the early morning hours. The exospheric temperature is derived from the Doppler line profiles and is compared to the topside F region O^+ temperature. The cooling of H relative to O^+ due to the escape of hot, energetic H is not obvious in our data, and it appears that a downward flux of hot protons often causes heating of the bound neutral H population by charge exchange during low to moderate solar activity conditions. This downward flux is usually strongest between 0200 and 0600 LT, and occurs throughout the night in the late fall and early winter. We have detected a deficiency of inbound high-energy hydrogen relative to the high-energy outbound population in radial velocity H_α profiles. We have also detected large distortions of the H_α profile wings during low to moderate solar activity periods and during periods of large downward ion speeds. We attribute these wing distortions to efficient charge exchange of H with H^+. A narrowing of zenith profile widths near midnight demonstrates the gravitational cooling of H due to the inverse relationship between geocentric distance and the kinetic energy required for escape. We have also searched for evidence that satellite hydrogen populations with small orbital eccentricities may be contributing to narrow line widths.

1. INTRODUCTION

Meriwether et al. [1980] demonstrated that technological advances made possible the retrieval of high resolution H_α profiles with a ground-based Fabry-Perot interferometer (FPI) at Arecibo, Puerto Rico. That investigation revealed the profile asymmetry related to hydrogen escape. The success of Meriwether et al. has motivated us to monitor the H_α line shape at several phases of a solar cycle. This paper deals with the observational results of six data-taking campaigns at Arecibo since 1980 (Table 1). Unfortunately, the 1981 campaign was plagued by poor weather conditions, and no results from that effort are presented.

The 6563 Å airglow is produced by the atomic hydrogen fluorescence ($3^2P_{3/2}$, $3^2P_{1/2} - 2^2S_{1/2}$) of solar Lyman beta (Ly β) photons in the geocorona [*Meier*, 1969]. Because the geocorona is optically thin at the H_α wavelength, the retrieved line profile is representative of the exospheric velocity distribution. The nature of this distribution as it pertains to the theory of the escape of light gases from planetary atmospheres has been widely discussed in recent literature [*Bertaux*, 1978; *Chamberlain*, 1963, 1976, 1977; *Donahue*, 1977; *Hodges et al.*, 1981; *Hunten*, 1973, 1982; *Hunten and Donahue*, 1976; *Liu and Donahue*, 1974a, b; *Maher and Tinsley*, 1977, 1978; *Fahr*, 1976; *Fahr and Paul*, 1976; *Fahr and Nass*, 1978; *Prisco and Chamberlain*, 1978, 1979; *Shizgal and Lindenfeld*, 1982; *Tinsley*, 1973, 1978; *Tinsley et al.*, 1975].

Paper number 5A8526.
0148-0227/86/005A-8526$05.00

A detailed description of current exospheric theory and its relationship to observations has been presented by *Fahr and Shizgal* [1983]. The observations presented here are used to investigate five primary topics relevant to exospheric theory. These are the exospheric hydrogen abundance, exospheric temperature, cooling due to the escape of energetic hydrogen (evaporative cooling), exospheric velocity distribution, and excitation of the H_α emission by multiply scattered solar Ly β radiation.

1.1 *Exospheric Hydrogen Abundance*

The measured H_α intensity depends upon the integrated abundance of hydrogen above the base of the emission cone and the solar Ly β flux. The base of the emission cone is defined as the intersection of the earth's shadow with the solid angle of the instrumental field of view. The nighttime variation of intensity measured in the zenith at Arecibo provides information on the distribution of hydrogen with altitude, since the base of the emission cone (shadow height) moves deeper into the geocorona as solar midnight is approached. Absolute intensities measured at similar shadow heights before and after solar midnight are compared to investigate asymmetry in the diurnal variation of critical level hydrogen density [*Tinsley et al.*, 1975; *Vidal-Madjar*, 1978; *Shih et al.*, 1985].

After adjustment that accounts for variation in the solar Ly β flux, absolute intensities may also be compared at various points along the solar cycle to determine variations of the exospheric hydrogen abundance related to solar activity [*Thomas and Anderson*, 1976; *Vidal-Madjar and Thomas*, 1978; *Shih et al.*, 1985].

The H_α intensity exhibits a linear relationship with hydrogen column abundance only if multiple scattering of solar Ly β

TABLE 1. Arecibo 6563 Å Data Taking Campaigns

Date	Duration, Days	Sensitivity, c/s/R	PMT	$F_{10.7}$	A_p
March 1980	7	0.66–1.0	RCA	137–154	1–5
April–May 1981	4	1.0	RCA	175–221	4–19
Oct.–Nov. 1983*	14	1.31	RCA	89–109	2–43
Dec.–Jan. 1983–1984*	15	1.01	RCA	81–95	3–33
April–May 1984*	9	1.99	Hamamatsu	113–183	6–72
Nov. 1984*	10	0.55	RCA	73–86	8–37

*Coincident radar measurements

photons into region below the illuminated emission cone may be neglected. Thus the diurnal and solar cycle variation of exospheric hydrogen abundance is best investigated when the observation geometry is such that we are looking directly into the sunlit region just above the exobase, as opposed to the situation when we are looking deep into the earth's shadow. Data taken in the twilight periods at Arecibo are most useful for determining diurnal and solar cycle variations of exospheric hydrogen abundance.

1.2 *Exospheric Temperature*

At the idealized exobase, or critical level for escape [*Chamberlain*, 1963], the hydrogen velocity distribution is assumed to have a complete Maxwell-Boltzmann distribution. The critical level is not so clearly defined in reality, and the region of transition between a collisional and noncollisional medium is not distinct. Symmetric H_α line profiles that originate from regions where collisions preserve a Maxwellian velocity distribution have a spectral width (FWHM) that is characteristic of the gas kinetic temperature. We have found that H_α profiles are usually indistinguishable from a Gaussian profile at or near the approximate critical level of 500 km. These symmetric profiles provide good estimates of the critical level temperature T_c [*Atreya*, 1973; *Atreya et al.*, 1975; *Kerr et al.*, 1984]. T_c is used in the parameterization of the thermal escape flux F_J, and the charge exchange escape flux F_{CE} [*Shizgal and Lindenfeld*, 1982]. T_c is also a common upper boundary condition in thermospheric models.

1.3 *Evaporative Cooling*

We have attempted to detect relaxational cooling of hydrogen relative to oxygen near the exobase due to the loss of the hot, energetic hydrogen component by escape [*Atreya*, 1973; *Fahr*, 1976; *Fahr and Paul*, 1976]. Simultaneous optical measurements of T_c and radar measurements of the nocturnal O^+ temperature in the topside F region were made in four periods beginning November 1983 (Table 1). The nocturnal O^+ temperature is expected to be close to the neutral thermospheric oxygen temperature [*Hanson and Carlson*, 1977].

1.4 *Line Profile Analysis*

As the velocity distribution becomes increasingly non-Maxwellian, the concept of the gas kinetic temperature loses its significance. The widths of the asymmetric profiles from the semicollisional regime above the exobase provide only an effective temperature [*Bertaux*, 1978], which is precisely a measure of the mean square velocity for exospheric hydrogen. As the base of the H_α emission cone increases in altitude, the H_α line profiles become distorted as a result of the nature of the exospheric hydrogen velocity distribution in the free flight gas regime. In sections 2 and 3 we briefly sketch the escape mechanisms important for terrestrial hydrogen and the manner in which exospheric line profiles may be distorted by varying populations of ballistic, escaping, and satellite hydrogen. Sections 2 and 3 serve as background for the presentation of our H_α temperature and line profile measurements.

1.5 *Multiple Scattering of Solar Ly β*

The possibility that multiply scattered Ly β photons may be exciting hydrogen emission at altitudes well below the base of an observer's illuminated emission column persists as a major caveat in the interpretation of H_α data (*Shih et al.* [1985] and J. Bertaux, R. Meier, and B. Tinsley, personal communications, 1984). Analysis of H_α intensity and line shape data is used to discuss this issue. A related problem is the uncertain determination of the base of the emission cone due to atmospheric screening.

It is our primary purpose in this paper to present observed H_α profiles for comparison with theoretical studies of the exospheric velocity distribution. Because detailed comparison to our data is beyond the scope of even the most comprehensive models [*Chamberlain*, 1976; *Bertaux*, 1978; *Prisco and Chamberlain*, 1978, 1979; *Hodges et al.*, 1981], only general conclusions are possible. The major unresolved problems that persist for modeling involve inclusion of the effects of multiple scattering and a consistent description of the satellite particle population. Nevertheless, the basic elements of current exospheric theory appear to be consistent with our observations.

2. TERRESTRIAL HYDROGEN ESCAPE

The idea of a region in the atmosphere where particle velocity distributions are no longer Maxwellian as a result of a transition from a collisional to a free flight gas regime was first explored by *Jeans* [1925]. His theory included an expression for the escape flux of hydrogen as a function of its temperature. The thermal escape flux of hydrogen increases exponentially with temperature:

$$F_J = \frac{[H]_c}{2(\pi)^{1/2}} \beta U(1+\lambda_c)\, e^{-\lambda_c} \tag{1}$$

where

$$\lambda_c = \frac{GMm_H}{kT_c r_c} \tag{2}$$

$$U = \left(\frac{2kT_c}{m_H}\right)^{1/2} \tag{3}$$

r_c geocentric distance at the exobase;
$[H]_c$ H number density at the exobase;
G gravitation constant;
M mass of the earth;
m_H mass of H atom;
k Boltzmann's constant;
T_c temperature at the critical level;

β adjustment factor depending upon ratio of masses of escaping gas to ambient atmosphere.

The concept of a limiting flux, due to the limited rate of supply of hydrogen to the exobase from below and caused by an effective diffusive barrier at the homopause, was first advanced by *Hunten* [1973] and was further discussed by *Hunten and Strobel* [1974] and by *Liu and Donahue* [1974*a*]. Their results indicated that the global escape flux was limited to a constant value of about 2.7×10^8 atoms $cm^{-2} s^{-1}$, equal to the upward flux of hydrogen from its mesospheric source.

Because the thermal escape flux of hydrogen at typical exospheric temperatures is found to supply only a portion of the allowed constant flux [*Liu and Donahue*, 1974a; *Bertaux*, 1975] and because the decrease in the density of hydrogen with increasing temperature is not observationally as pronounced as expected from thermal escape considerations alone, another escape mechanism is needed. *Tinsley* [1973] and *Tinsley et al.* [1975] showed that the resonant charge exchange reaction of *Cole* [1966]:

$$H + H^+_{hot} \rightarrow H_{hot} + H^+ \quad (4)$$

makes a significant contribution to the escape flux as a result of the creation of hot hydrogen atoms with sufficient kinetic energy to escape. Since (4) proceeds most efficiently in the exosphere, there may be significant escape of energetic H before the inverse reaction occurs. Reaction (5) can also create H with sufficient energy for escape. However, (5) proceeds most efficiently in the thermosphere, where the proton temperature is lower, and the inverse reaction will take place rapidly. Also, collisions in the thermosphere preserve near-thermal equilibrium between H and O [*Tinsley*, 1978].

$$H^+ + O \rightarrow H + O^+ \quad (5)$$

As T_c increases, the charge exchange escape flux decreases as a result of the lower abundance of hydrogen available for collisions. Thus the charge exchange flux decreases in importance relative to F_J with increasing exospheric temperature, and vice versa. At 900 K and 1200 K, F_J accounts for 10 and 65% of the total flux, respectively [*Hunten and Donahue*, 1976].

Subsequent studies revealed that the charge exchange reaction (equation (4)) would affect exospheric hydrogen in each trajectory classification: ballistic, hyperbolic, and elliptic orbiters (satellites). The impact on the overall velocity distribution has been investigated by *Chamberlain* [1977], *Maher and Tinsley* [1977, 1978], *Tinsley* [1978], *Prisco and Chamberlain* [1978], and *Hodges et al.* [1981], as well as others.

Hyperbolic escaping trajectories are created when the H^+ energy exceeds that necessary for H escape, and the direction of the hot H^+ prior to collision is upward. If the ion direction is downward, the energetic neutral created by collision moves in a ballistic trajectory that intersects the exobase, where subsequent collision with neutrals enhances the mean velocity (temperature) of the bound population. Some energetic hydrogen directed toward the exobase is reflected by collision. This upward "splash" [*Chamberlain*, 1977] contributes to the escape flux.

The existence of a significant satellite population was predicted on the basis of occasional collisions in the exosphere that redirect hydrogen into long-lived, stable orbits [*Chamberlain*, 1963]. The most likely collisional partner for H in the exosphere is H^+ [*Chamberlain, 1963; Maher and Tinsley*, 1977; *Chamberlain*, 1979; *Prisco and Chamberlain*, 1979]. However, *Maher and Tinsley* [1977] have pointed out that satellites will be destroyed and created by charge exchange at roughly the same rate. This implies that the satellite population will be proportional to the neutral hydrogen density, since the other two primary sources of satellites are neutral-neutral collisions and solar Ly β radiation pressure [*Maher and Tinsley*, 1977]. The primary sink for satellites above the plasmapause is radiation pressure, which acts selectively to eliminate satellites of high eccentricity [*Bertaux and Blamont*, 1973; *Bertaux*, 1978; *Donahue*, 1977; *Chamberlain*, 1979]. Additional discussion regarding the variation of satellite particle population with altitude and the solar cycle can be found in section 3. In any event, various estimates have indicated that the satellite population may comprise as much as 35–55% of the entire exospheric hydrogen inventory [*Chamberlain*, 1963, 1977; *Bertaux*, 1978; *Hodges et al.*, 1981].

The charge exchange reaction (equation (4)) has a total cross section that is only a weak, logarithmic function of temperature [*Maher and Tinsley*, 1977; *Shizgal and Lindenfeld*, 1982], and the rate at which it proceeds in the earth's geocorona is most strongly dependent upon [H] and $[H^+]$. On the other hand, the flux of escaping particles generated by charge exchange is proportional to the proton temperature T_{H^+}. As T_{H^+} increases, more collisions result in neutral hydrogen with escape velocity. This intuitive conclusion has been substantiated by an analytic expression for the escape flux, which was developed by *Shizgal and Lindenfeld* [1982].

$$F = [H^+]_e (2KT_c/m_H)^{1/2} e^{-\lambda_c} [(1 + \tau) - (1 + \tau)^{-1/2} e^{-\tau\lambda_c}]/\tau \quad (6)$$

Here $\tau = (T/T_{H^+}) - 1$, $[H^+]_e$ is the effective proton number density as defined by *Shizgal and Lindenfeld* [1982], and the other parameters are defined in (3). The increase of F_{CE} with T_{H^+} is also evident in the Monte Carlo model of *Hodges et al.* [1981].

Analysis of (6) shows that F_{CE} increases rapidly with increasing T_{H^+}, and that F_{CE} increases relative to F_J (1) for decreasing T_c and constant T_{H^+}. Clearly, as T_{H^+}/T_c increases, the population of satellites relative to the population of hydrogen on escaping trajectories will diminish, as a result of the additional kinetic energy imparted to the neutral hydrogen following the collision (4). This reduction in the satellite population relative to escaping particles apparently preserves the nearly stable population of satellites with respect to exospheric hydrogen [*Hodges et al.*, 1981].

The dependence of F_{CE} on T_{H^+} and $[H^+]$ (equation (6)) may result in local perturbations of the diurnal and solar cycle variations in exospheric [H]. *Vidal-Madjar and Thomas* [1978] suggest that an early morning, mid-latitude depletion of atomic hydrogen measured by satellites D2A [*Emerich et al.*, 1976; *Emerich and Cazes*, 1977] and OGO 6 [*Thomas and Anderson*, 1976] may be due in part to an increase in F_{CE} near the morning terminator.

A detailed analysis of data from the Arecibo radar facility and the OGO 6 and AE-C satellites by *Maher and Tinsley* [1977, 1978] and *Tinsley* [1978] has been made to study the variation of F_J, F_{CE}, and the escape of H in the form of H^+ at middle and high latitudes (F_{IL}). Their results suggest that these fluxes vary in a more complex manner than had been described previously [*Hunten and Donahue*, 1976], so that both F_{CE} and F_J increase for low to moderate values of the solar flux, while F_{IL} decreases rapidly to preserve the constant global flux. *Maher and Tinsley* [1977] argue that such a variation might be expected in view of the dependence F_{CE} on $[H^+]$ and T_{H^+}, both of which increase with solar activity. For moderate to high solar activity, F_{IL} becomes

negligible, while F_J increases and F_{CE} decreases [*Maher and Tinsley*, 1978].

Other modes of escape (such as H^+ loss in the polar wind) have been described by *Hunten* [1982], *Thomas and Vidal-Madjar* [1978], and *Tinsley* [1978]; these have second-order effects at Arecibo. While these other modes are generally not observable at Arecibo, they do affect the exospheric hydrogen distribution. *Thomas and Vidal-Madjar* [1978] have shown that a distinct latitudinal gradient in the hydrogen density, especially at solstice, implies a greater escape flux at the poles than near the equator. In other words, the constant global escape flux may be supplied preferentially in the polar regions, with a smaller contribution from the equatorial zone. Another cause of this latitudinal gradiant may be exospheric winds [*Vidal-Madjar*, 1978].

3. Exospheric Line Profiles

It is evident from the preceding discussion that unraveling the mechanisms which contribute to any particular geocoronal H_α profile is not a trivial matter. Nevertheless, high spectral resolution profiles may be compared qualitatively to the theoretical profiles of *Chamberlain* [1976], *Bertaux* [1978], *Prisco and Chamberlain* [1978, 1979], and *Hodges et al.* [1981] to determine which processes are having primary impact upon the exospheric velocity distribution at any time.

The kinetic energy required for hydrogen escape decreases with geocentric distance r, since the escape velocity v_{esc} is inversely proportional to r

$$v_{esc} = [2GM/r]^{1/2} \tag{7}$$

The parameters in (7) are the same as defined in (2). So to a first order of approximation a narrowing of line widths with increasing shadow height is expected, due to the earth's reduced capacity to retain energetic hydrogen as geocentric distance increases [*Bertaux*, 1978]. This effect, known as gravitational cooling, is related to but distinct from thermal escape. This first-order narrowing may be masked by other processes that perturb the exospheric velocity distribution.

There is a distinction between the effects we refer to as gravitational and evaporative cooling. Gravitational cooling is the symmetric narrowing of the emission profile with geocentric distance. Evaporative cooling refers specifically to the difference between hydrogen and oxygen temperatures near the exobase.

Thermal escape modification of the velocity distribution introduces a population of escaping or hyperbolic trajectory particles. These particles appear in the outbound energetic tail of the radial velocity distribution. However, the short-wavelength (incoming) wing of the airglow profile observed in the zenith will appear depleted, since the earth is unable to capture and retain interplanetary hydrogen with these energies. In other words, the population of the outbound hyperbolic particles is greater than inbound particles of the same energy. This effect was first witnessed at H_α by *Meriwether et al.* [1980], and is shown here in Figure 1*b*.

The clearest evidence of gravitational cooling and the line asymmetry due to thermal escape will be seen in H_α profiles obtained during periods of moderate to high solar activity. The diminished importance of charge exchange during these periods should result in minimal perturbations of the velocity distribution wings by the presence of energetic H created by (4). Also, the thermal escape flux is greatest during active solar periods.

The most obvious distortions of geocoronal line profiles occur when charge exchange proceeds efficiently. *Hodges et al.* [1981] have generated theoretical profiles that indicate that the outbound hyperbolic (red) wing is enhanced when $T_H+ > T_H$ (T_{H+} increasing with altitude), relative to the case when no H^+ is present. Furthermore, the altitude profiles of proton density and temperature adopted by *Hodges et al.* [1981] result in some filling in of the incoming (blue) side of the radial velocity profile. Efficient charge exchange with a very hot proton population ($T_{H+} = 5000$ K) may create more significant distortions in the profile wings than those presented in the Hodges et al. study.

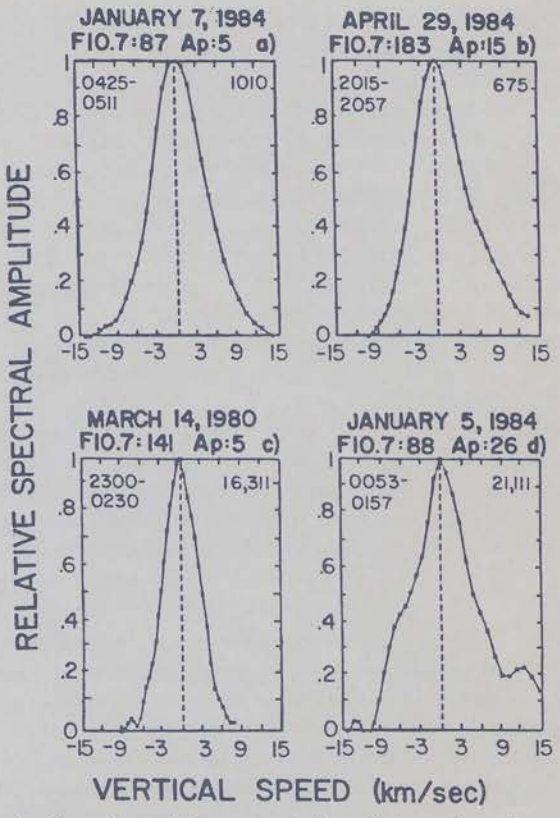

Fig. 1. Four H_α profiles representative of those often observed at Arecibo. (*a*) A complete Maxwell-Boltzmann velocity distribution. (*b*) A distribution showing the asymmetry between outbound and inbound hydrogen. (*c*) A narrow profile of the type often detected near solar midnight. (*d*) A broad, shouldered profile that is also common. Each profile includes the solid earth shadow height at the time of observation to the right of line center and the local time period of data summation to the left. Negative velocity represents incoming hydrogen, while positive velocity represents outbound hydrogen, moving away from the observer. These profiles include the FPI instrument function and have been normalized to unity at line center intensity.

Evidence of charge exchange in the measured profiles should be most pronounced below the plasmapause and specifically within the region spanning just below the exobase to about 2500 km [*Hodges et al.*, 1981; *Shizgal and Lindenfeld*, 1982]. The Monte Carlo technique of Hodges et al. showed that the affect of charge exchange on the incoming side of the radial velocity distribution nearly disappears at altitudes greater than about 10^4 km (2.6 earth radii, R_E). *Shizgal and Lindenfeld* [1982] stated that only about 5% of the charge exchange escape flux is contributed from altitudes above 3000 km (1.5 R_E).

In summary, the affects of charge exchange on geocoronal H_α profiles may be most evident during periods of low to moderate solar activity and for observations with the shadow heights between about 500 km (1.1 R_E) and 10^4 km (2.6 R_E). The presence of a red/blue radial profile asymmetry below 2 R_E may be masked by filling in of the incoming (blue) energetic wing due to the creation of incoming energetic hydrogen by charge

exchange. The asymmetry should slowly reappear as the shadow height increases in altitude toward 2.6 R_E. The creation of energetic hydrogen with inbound and outbound velocities in excess of the escape velocity appropriate for a certain altitude (equation (7)) may also be evident in the profile wings.

Where and when satellite hydrogen populations will be evident in geocoronal line profiles is not clear. Indeed, there is substantial ambiguity in theoretical descriptions of the satellite particle distribution [*Bertaux*, 1978; *Prisco and Chamberlain*, 1979]. A treatment which examined the change of line shape features with increasing satellite population has been presented by *Prisco and Chamberlain* [1979].

Because residence times in the orbiting population are on the order of days, large satellite hydrogen populations may be established without collisions between H and H^+ but by the transfer of momentum in Ly α photon scatter [*Hodges et al.*, 1981]. Some contribution to the satellite population is also made by rare neutral-neutral collisions. Orbits created by Ly α momentum transfer (radiation pressure) will have large eccentricities, since the most likely candidate for orbit insertion would be a particle with an initial outbound velocity near to the escape velocity and therefore a long flight path along which the momentum transfer may occur [*Hodges et al.*, 1981].

As has been described earlier, charge exchange is an effective source of satellite particles. Although charge exchange also represents the primary sink for satellites in the plasmasphere [*Maher and Tinsley*, 1978], there may be a slight enhancement of the satellite particle population relative to the entire exospheric H inventory when charge exchange proceeds efficiently. The model of *Hodges et al.* [1981] shows that the ratio of orbital insertion to ballistic trajectories in the no H^+ case is a factor of 5 less than that when H^+ is included in the model but that the inclusion of H^+ enhances the population of satellites relative to all hydrogen in the exosphere by only 8%.

Intuitively, it seems that the detection of a satellite particle population would be slightly more likely for observations made during low to moderate solar activity conditions, when charge exchange proceeds most efficiently. This is consistent with the suggestion of *Maher and Tinsley* [1978] that the satellite population is expected to be proportional to the neutral density at the exobase, for a first approximation. This density will be the largest at solar minimum.

An important loss process for satellites, especially above the plasmapause, is the systematic lowering of satellite perigees by solar radiation pressure. When perigees are driven below the exobase, collisions effectively terminate satellite trajectories. This process has been modeled by *Bertaux and Blamont* [1973], *Bertaux* [1978], and *Chamberlain* [1979]. Generally, these studies agree that satellites with high eccentricities will be preferentially depleted and that orbits with low eccentricity will dominate the satellite population. Primary differences between the models of Bertaux and Chamberlain appear in the spacial distribution of satellites with respect to the ecliptic plane and the earth-sun line.

Ly α absorption cell data from satellite OGO 5 have been used to determine the vertical distribution of satellite particles by *Bertaux and Blamont* [1973] and *Bertaux* [1978]. On the dayside, they find the satellite concentration is insignificant below 2 R_E, is greatest at 3 R_E, and rapidly decreases above 7 R_E. This is contrary to the concept of a well-defined satellite critical level, below which no satellite perigees exist. The satellite critical level is a useful concept for computation of exospheric density [*Chamberlain*, 1963] but may not be physically realistic. A satellite critical level at 2.5 R_E is adequate to explain OGO 5 nightside data [*Bertaux*, 1978]. These satellite distributions have been disputed as nonunique interpretations of the OGO 5 data by *Prisco and Chamberlain* [1979]. It appears that some variation in the satellite population with altitude is to be expected, since most satellites will have low orbital eccentricities.

The contribution of a low-eccentricity hydrogen satellite population to radial velocity profiles will occur at line center, since particles in circular orbits have zero radial velocity. *Prisco and Chamberlain* [1979] have shown that radial geocoronal line profiles from distributions that include a large satellite population are therefore highly peaked and narrow, and depressed in the line wings (as in Figure 1*c*). Normalized profiles that are narrow at the peak but broad at the half height may result from smaller satellite populations [*Prisco and Chamberlain*, 1979]. These shouldered profiles may be physically interpreted as the result of a measurable satellite population imposed upon the broad wings of a profile characteristic of a hot ballistic component. An example of a shouldered profile is shown in Figure 1*d*.

A further complication with respect to the interpretation of line profiles is that a satellite particle will have a temperature characteristic of the hot ion that created it, which may be very different from the temperature of the remaining hydrogen distribution. Depending upon the residence time of particles in satellite orbits, it is also possible that a multimodal temperature distribution may be established among the satellites [*Prisco and Chamberlain*, 1979; *Hodges et al.*, 1981].

Although speculative, it seems that the spectral signature due to emission from satellite particles would most likely be detected during low to moderate solar activity periods and for shadow heights between about 2 R_E and 6 R_E. Since satellites are gravitationally bound and may not have radial velocities greater than that for escape, the escape velocity may be used to isolate features that may be due to a satellite population. For example, Figure 1*c* shows a highly peaked profile depressed in the wings, which may be due to a large satellite particle population, or it may simply illustrate the effect of gravitational cooling at great altitude [*Bertaux*, 1978]. By determining the velocity of escape appropriate for the shadow height, these two possibilities may be investigated more thoroughly. If it is found that the profile of Figure 1*c* falls well within the escape velocity limit, then it may indeed be the signature of a significant satellite population. Alternatively, if truncation of the profile wings is coincident with the escape velocity, the narrow profile is probably the result of gravitational cooling in the outer geocorona. Similarly, the shouldering illustrated in Figure 1*d* is constrained to occur within the limit of the escape velocity in the event that satellite particles are causal, while enhancements in the profile wings due to charge exchange with very energetic protons are not subject to the same constraint. It should be stressed that such an analysis is only sensible in the event that the instrument function is removed from the data in a manner that preserves the detail of the actual emission function. Such a procedure has been developed for the purpose of profile and temperature analysis and will be described in section 6. The profiles of Figure 1 retain the FPI instrument function.

4. INSTRUMENTATION

The Fabry-Perot interferometer used to measure geocoronal H_α at Arecibo was configured in the same manner as described by *Meriwether et al.* [1980]. The time evolution of the sensitivity at H_α is shown in Table 1. The sensitivity improved by a factor of 25 between 1973 and 1980 and by a factor of 3 between 1980

and 1984. The lower sensitivity of the November 1984 period (Table 1) is due primarily to the use of a photomultiplier tube (PMT) with half the quantum efficiency of the one used in April 1984. The interference filter currently in use has 75% transmission and a 6.9 Å spectral width. Also, the quantum efficiency of the currently installed Hamamatsu Ga-As red sensitive photomultiplier is approximately 16%. While this tube employs a larger cathode area than the RCA tubes used previously, the dark count at 50°C remains at about 1 count s^{-1}.

Calibration of the instrumental function with a He–Ne frequency stabilized laser has indicated an overall instrumental finesse between 9.5 to 11.5, varying slightly between observation campaigns. A finesse of 13.0 was achieved during the 1980 campaign. The effective resolving power of the FPI is about 6.36×10^4, giving a spectral resolution of 0.075 Å at H_α.

Absolute intensity calibration is achieved via cross calibration with a tilting filter photometer, which is calibrated with a ^{14}C constant brightness source. The accuracy of these calibrations is estimated to be no worse than plus or minus 25% for those periods after the 1981 campaign, and no worse than plus or minus 35% for the 1980 and 1981 observing periods [*Meriwether et al.*, 1980].

The incoherent scatter radar at Arecibo was used to measure *F* region autocorrelation functions (ACF) and power profiles in an alternating manner. The ACFs, from which we derive temperatures, were sampled in 12-km intervals between 160–650 km, for about 1 min per altitude profile. Off-line averaging degraded the time resolution per altitude profile to about 10 min. Radar temperatures at 400 km are accurate to plus or minus 20 K.

5. OBSERVATIONS

We chose to observe at Arecibo, Puerto Rico, for several reasons. Most importantly, simultaneous radar measurements of the topside *F* region are available. The location of the observatory (18.35°N, 66.75°W) also allows for optical line of sight zenith measurements to extremely large shadow heights. This allows for altitude coverage from a few hundred kilometers to 20 R_E during winter observing periods. Arecibo is also advantageous for measurement of H_α because its subtropical location minimizes the possible effects of high energy (>10 eV) charged particle precipitation. While the effect of such precipitation is interesting in itself, the possibility that other hydrogen fine-structure transitions may be collisionally excited by particle precipitation would confuse the line profile interpretation [*Yelle and Roesler*, 1984, 1985].

Our strategy has been to observe in the zenith during new moon periods between the late fall and early spring. The zenith observations represent the simplest viewing geometry and have the advantage of directly supplying vertical velocities in the line of sight. Tropospheric scattering of H_α into the observation cone is smallest for zenith observations [*Shih et al.*, 1985]. Furthermore, this geometry allows for the most direct comparison of the H_α line shapes to theory. The winter months are stressed, since this period allows for optical measurements in the zenith deep into the geocorona. In practice, zenith observations were not always possible, since galactic H_α emissions must be avoided. In all cases, measurements were within 15° of the zenith, however. The radar measurements were always made in the same direction as the interferometer.

There are several sources of potential contamination, namely emissions of H_α from nongeocoronal sources. These are detailed by *Atreya* [1973] and include the gegenschein, the zodiacal light, interplanetary H_α, and the galactic emission. Since the maximum intensity of interplanetary H_α is calculated to be no greater than 0.1 R [*Atreya*, 1973], the most insidious source of contamination has proven to be galactic H_α. Arising from hot H II regions and the interstellar medium in the galactic spiral arms [*Reynolds et al.*, 1973], galactic H_α is much broader than the geocoronal emission and usually has a large Doppler shift away from the geocoronal emission. The intensity varies from a few tenths of a rayleigh to hundreds of rayleighs, and the emission is generally constrained to approximately plus or minus 30° galactic latitude.

Galactic emission with great intensity or large Doppler shift is easy to detect in our line profile measurements. Still, there are occasions when galactic H_α appears as a weak broad background with a slight Doppler shift and is difficult to detect. We attempted to avoid H_α emissions in the region 30° on either side of the galactic equator. When this was not possible we used the galactic maps of *Reynolds et al.* [1973, 1974] and *Reynolds* [1983] to avoid galactic contamination. Unless otherwise stated, galactic contamination was not present in any of the results reported here.

Another potential for contamination at H_α is the nearby OH(6–1), P branch rotational lines at +6.2 Å and −9.1 Å [*Atreya*, 1973]. These lines are precluded from geocoronal H_α contamination by the characteristics of the triple-cavity interference filter, which has greater rejection in the wings than a filter with a Gaussian passband.

Typically, the H_α line profile measurements consist of 35 points with 10-s integration time at each point, so that a fringe is obtained in less than 6 min. Pressure changes generated the fringe scan by changing the density of the gas between the etalon plates.

6. ANALYSIS

Examples of two unprocessed FPI sky fringes are shown in Figure 2. The low signal to noise ratio near solar midnight requires integration of several fringes prior to more detailed analyses of intensity, temperature, and line shape.

Intensity

After summing achieves good signal over noise profiles, a fitting function derived from a Gaussian is applied to the fringe. An amplitude, peak position, background, and profile width are

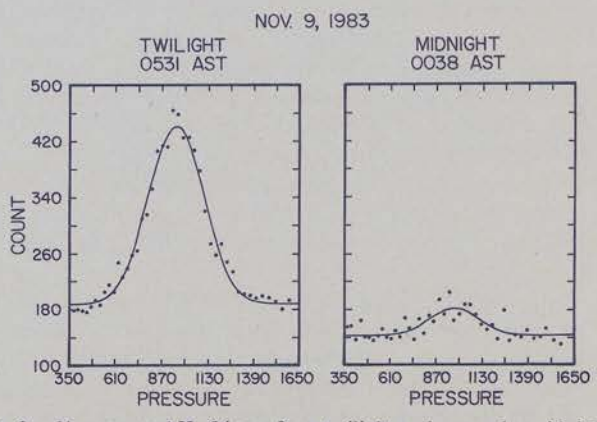

Fig. 2. Unprocessed H_α fringes from twilight and near solar midnight. Each point along the pressure scan is integrated for 7.5 s, giving a total of 5.25 min of integration for each fringe. A Gaussian function has been fit to the data using the method of nonlinear least squares and is shown by the solid line.

determined by means of nonlinear least squares. Absolute intensity is determined by applying a calibration sensitivity factor.

Temperature and line shapes

The asymmetric velocity distribution of exospheric hydrogen, due to breakdown of the hydrostatic law, results in a poor determination of the H_α profile width by the fitting procedure just described. To achieve a more accurate determination of line widths and isolation of the source function, a Fourier deconvolution scheme has been developed. This scheme removes the instrument function from the measured FPI output function, which is the physical convolution of the instrument function and the source function. The method makes no assumption about the shape of the instrument function or the shape of the emission profile. In this way an emission function is obtained that preserves the finer details of the measured profile.

A detailed description of the deconvolution procedure will be reserved for a later paper, but the basic features are as follows. After summing individual fringes to improve signal over noise, a three-point running average is performed on the data, and the background determined by the Gaussian fitting procedure is removed. A 15-term Fourier series is then fit to the profile, again using the method of nonlinear least squares. The Fourier series is calculated by assigning the characteristic FPI interval of one free spectral range to the characteristic Fourier interval, 0 to 2π. Since data is taken over a narrower spectral region than one free spectral range (FSR) to preserve temporal resolution, the fringe is extended artificially to one FSR by extrapolating points that are equal to the background value.

By including 15 terms in the Fourier-fitting procedure (both symmetric and asymmetric terms) we have been able to reproduce the measured profile shape with great accuracy. Line center is determined by the peak of this Fourier fit, which we find to be much more accurate than line center determination using a Gaussian function. This has been confirmed by comparing the position of line center, as defined by the peak of the Fourier function, to the unambiguous line center determined by a hydrogen spectral lamp calibration [*Atreya*, 1973].

After fitting the data with a Fourier series function and determining line center, the profile is normalized to unity at the peak position. The result is a function that accurately describes the FPI output function and makes no assumptions regarding its shape.

The instrument function is measured by passing light from a He-Ne frequency-stabilized laser through the etalon plates. These calibration spectra are analyzed in a similar manner. No smoothing of the measured profile is necessary. We have found that as many as 25 Fourier terms are sometimes required to achieve a satisfactory fit to the peak of a laser calibration.

The pure source profile is determined by deconvolving the instrument function from the FPI output function according to the Fourier convolution theorem. This requires calculation of the respective discrete Fourier transforms, complex division of the output transform by the instrument transform, and filtering of the resultant transform. After adjustment for the phase shift between Fourier and real space, the final form of the deconvolved transform is inverted to obtain the pure source function.

The emission function we measure is systematically broader than that characteristic of the exospheric velocity distribution because the measured emission is actually an unresolved two-line emission (see appendix). This has been accounted for in our analysis by convolving the measured instrument function with a synthetic, symmetric function that takes account of the systematic broadening. The resultant function is then used as an effective instrument function for the deconvolution. It is shown in the appendix that the two H_α fine-structure lines remain completely unresolved for the full range of temperatures and spectral resolutions appropriate for the data presented here. Thus the line shape is altered to account for the fine structure of geocoronal H_α without obscuring the subtleties of profile structure, and the FWHM of the pure emission function is characteristic of the actual exospheric radial velocity distribution.

To determine the effective temperature, the source function red side half width at half height is added to the blue side half width, giving an effective FWHM. The effective temperature is then calculated from

$$T = \frac{FWHM}{(21n2)^{1/2}} \frac{c^2}{\lambda_o^2} \frac{m_H}{2k} \tag{8}$$

where c is the velocity of light, and λ_o is the wavelength of the H_α emission. Other parameters are defined in (3).

7. RESULTS AND DISCUSSION

Exospheric Hydrogen Abundance

Figure 3 shows the absolute intensity variation of H_α at Arecibo for a collection of dates when the best data have been obtained. These absolute intensities may be normalized with respect to the solar Ly β flux at solar minimum, following the procedure of *Shih et al.* [1985]. The solar Ly β flux is related to the $F_{10.7}$ cm flux by

$$R_{L\beta} = B_0 + B_1 (F_{10.7} - 71.5) + B_2 (F_{10.7} - \bar{F}_{10.7} + 3.9) \tag{9}$$

where

$\bar{F}_{10.7}$ daily mean solar 2800 mHz flux
$F_{10.7}$ three solar rotation average $F_{10.7}$
B_0 1.31
B_1 0.01106
B_2 0.00492

[*Shih*, 1983; after *Hinteregger*, 1981]. Normalized intensities are obtained by dividing the absolute measured intensities by the $R_{L\beta}$ factor appropriate for the observation period. The result of this normalization is shown in Figure 4, where the intensity variation now reflects the actual variation in hydrogen column abundance, to within the limits of accuracy of (9).

Figure 4 shows a slightly greater variability of exospheric hydrogen abundance in the morning hours than during the evening hours. The spread of normalized intensities in the morning twilight data implies an actual variation in hydrogen column abundance above the exobase of nearly 250% for our observations. Comparison during the twilight periods is cogent, since the effect of multiple scattering is minimal during this period, when the observations are made looking directly into the illuminated region.

Quadratic fits to the normalized intensities measured at four periods of the solar cycle since 1980 are presented in Figure 5.

$$I = a_0 + a_1(\log z) + a_2 (\log z)^2 \tag{10}$$

Here, I is intensity, z is the solid earth shadow height in kilometers, and a_0, a_1, and a_2 are the quadratic coefficients. In each case, two fits have been calculated, one for the morning (postsolar midnight) intensities, and one for the evening (presolar midnight) intensities. Figure 5 does not contain a curve for the April–May, 1984 campaign because a remarkable enhancement of intensity occurred after April 24, 1984. For this reason, two sets of quadratic fits have been calculated describing the

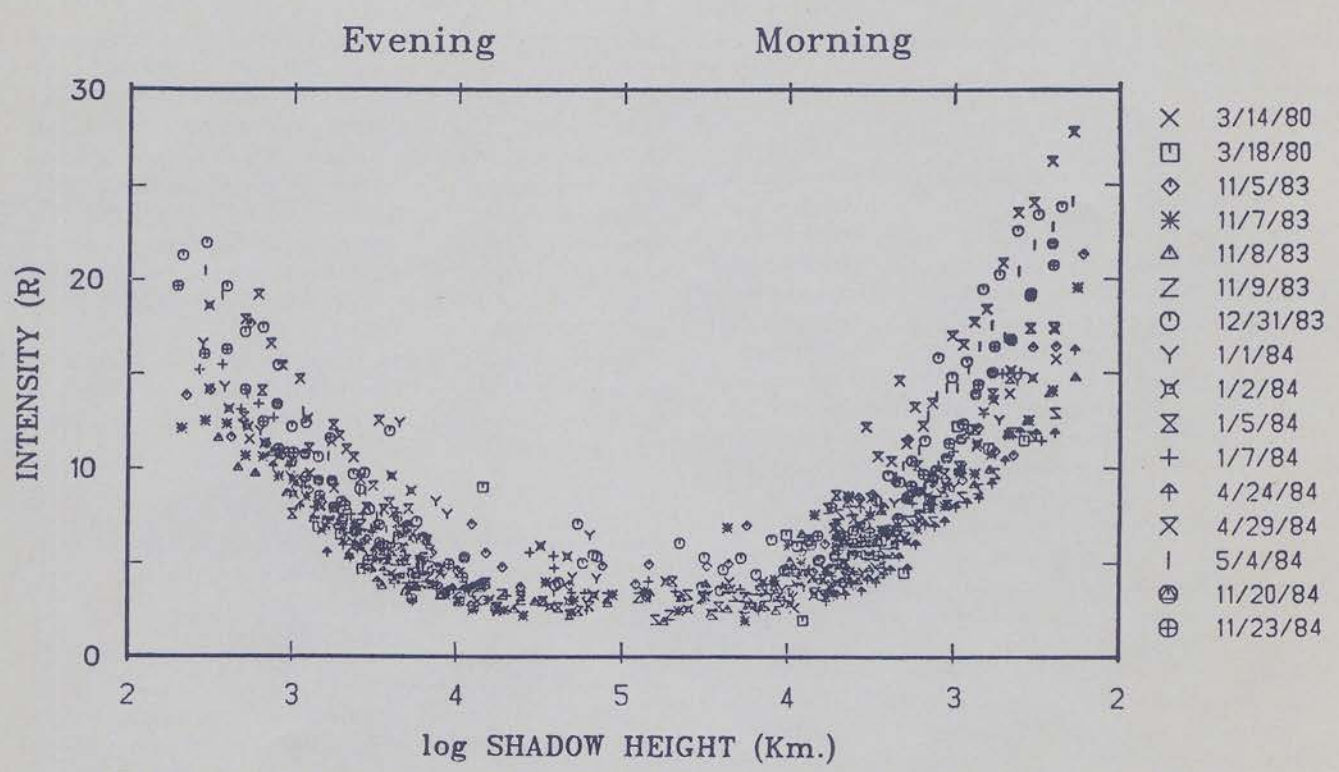

Fig. 3. Absolute H_α intensities for various dates including five observation periods. The abscissa is $\log_{10}$ of the solid earth shadow height.

disparate intensity measurements obtained during this period. Table 2 contains the quadratic coefficients for each period, where the fit has been applied to those dates included in the legend of Figure 4. The results for each campaign appear highly symmetric about solar midnight.

Using the calculated quadratic coefficients (Table 2), intensities normalized to the solar Ly β flux at solar minimum may be calculated for any shadow height, and this intensity is proportional to the hydrogen column abundance. We will argue in a later section that multiple scattering contaminates our data

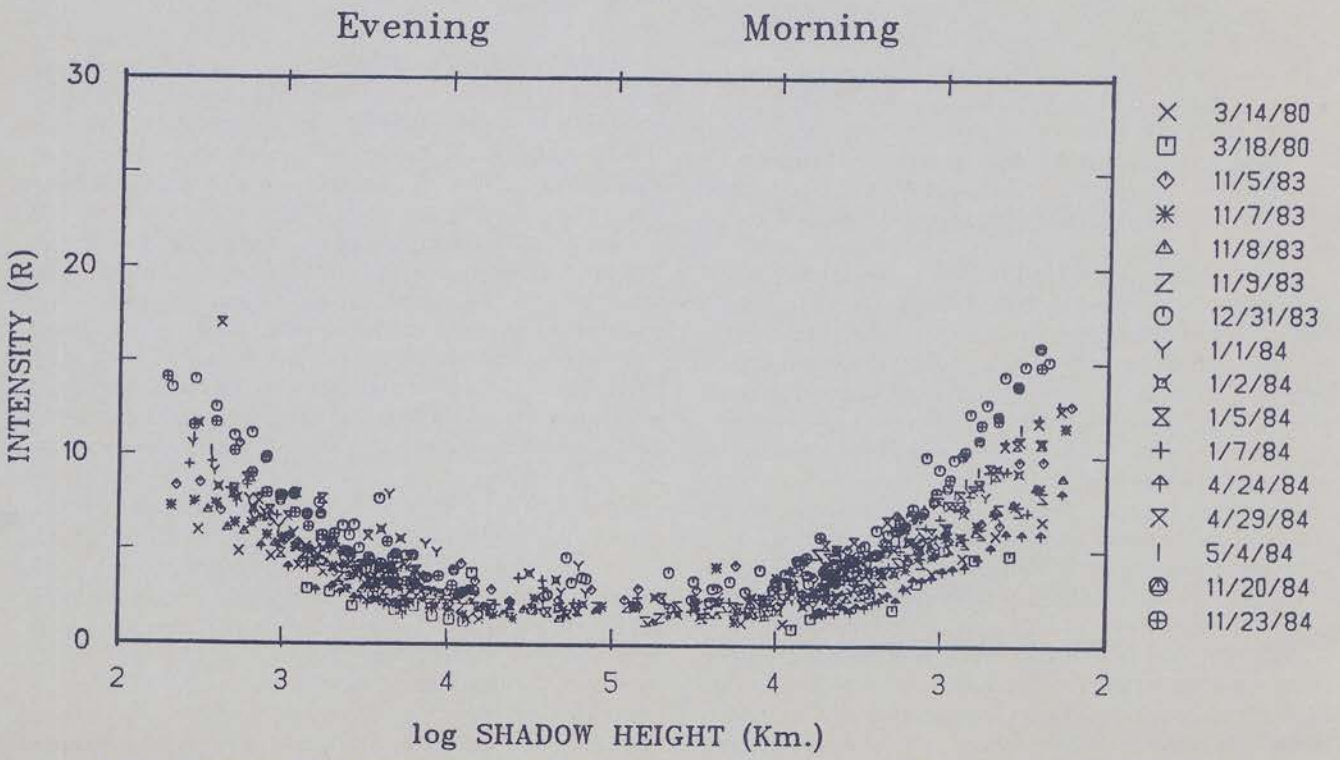

Fig. 4. The same as Fig. 3, except that the intensities have been normalized with respect to the solar minimum Ly β flux. The normalization procedure is described in the text.

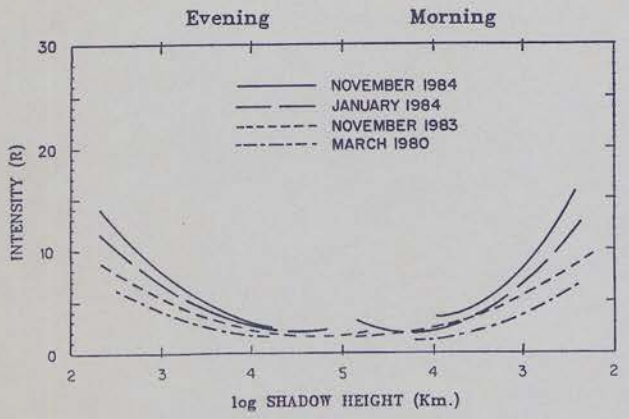

Fig. 5. Reduced chi-square quadratic fits to the intensities which have been normalized to solar minimum Ly β flux conditions. Each fit corresponds to the data collected for one observation period; the dates included are listed in the legends of Figures 4 and 5.

significantly only for shadow heights above about 5 R_E.

On the basis of OGO 6, OGO 5, and OSO 5 satellite data, *Thomas and Anderson* [1976] developed an empirical relationship for the number density at the exobase as a function of T_c.

$$[H]_c = \frac{1.93 \times 10^4 \exp[7029/T_e]}{T_e^{1/2}[1 + 7029/T_e]} \text{ cm}^{-3} \quad (11)$$

where

$$T_e = b_1 + b_2 T_c \quad (12)$$

and

$$b_1 = 475 \qquad b_2 = 0.525$$

Vidal-Madjar [1978] reanalyzed the empirical fit by including data near solar minimum from satellites OSO 5, AE-C, and Explorer 32. This analysis also made use of a determination of [H] at 500 km by *Ho and Moorcraft* [1971] and a moderate solar activity data point from the French D2A satellite. *Vidal-Madjar* [1978] asserted that the coefficients b_1 and b_2 (equation (12)) of *Thomas and Anderson* [1976] underestimate the hydrogen density for low solar activity conditions and derived values of b_1=363 and b_2=0.640.

Shih [1983], and *Shih et al.* [1985] extended the empirical relation (equation (11)) to estimate column abundance above an arbitrary altitude for comparison with ground-based H_α observations. The relationship for column abundance is

$$L = \frac{[H]_c k T_c}{m_H g(r)} \exp\left(\frac{N}{T_c}\right) \quad (13)$$

The exponent accounts for the decrease in [H] with geocentric distance on the basis of hydrostatic equilibrium, where

$$N = \frac{GMm_H}{k}\left(\frac{1}{r} - \frac{1}{r_c}\right) \quad (14)$$

The value of N is −477 at 1000 km and −101 at 600 km.

Nighttime variation. Table 3 lists $\bar{F}_{10.7}$, $F_{10.7}$, and the value of $R_{L\beta}$ from (9) for six periods since 1980. The ratio of morning intensity to evening intensity after adjustment for the Ly β flux is R_{NI}. This ratio has been calculated by determining the intensity at similar solid-earth shadow heights in the morning and evening and dividing the respective values. Each intensity may be calculated using the quadratic coefficients of Table 2 in (10). The ratio of morning to evening column abundance, R_{NI}, above a solid earth shadow of 600 km or 1000 km is nearly equal to 1.0 at Arecibo (Table 3).

Because of the column-integrated nature of our data, it is difficult to compare our results with models and previous observations of the number density at the exobase. Although (13) does not account for various fluxes in the exosphere that may have profound affects on the column abundance, it may be used to provide a rough estimate of the column abundance above altitudes not far removed from the exobase. Ratios of morning to evening column abundance based on the diurnal $[H]_c$ model of *Tinsley et al.* [1975] and the data from satellites D2A [*Emerich et al.*, 1976; *Emerich and Cazes*, 1977] and OGO 6 [*Vidal-Majar*, 1978] are shown in Table 3.

Tinsley et al. [1975] modeled the diurnal variation of $[H]_c$ by including the diurnal variation of the F_{CE}, F_J, a rotating thermosphere with local temperature variations, and transport due to winds. The result was a sinusoidal diurnal variation in $[H]_c$, with a maximum at about 0400 and a minimum at about 1600 LT. The ratio of maximum to minimum $[H]_c$ varied between 1.26 and 2.97 for the range of conditions analyzed. The ratios of morning to evening $[H]_c$ calculated by this model for conditions similar to our data are listed in Table 3 as R_{TIN+} and R_{TIN-}. R_{TIN+} represents the largest ratio within the limits of the model results, while R_{TIN-} is the smallest. If the temperature at the exobase is the same for both morning and evening observing periods, the ratio of column abundances estimated by using (13) is equal to the ratio of morning to evening $[H]_c$, since the scale height and the exponent of (13) are unchanged. The ratio of morning to evening column abundance using the critical level temperature calculated by the mass spectrometer/incoherent scatter (MSIS) model [*Hedin*, 1983] is also listed in Table 3, as is the ratio using our measured value of T_H. In determining the column abundance from exobase number density, the altitude corresponding to the base of the emission column was estimated by including a 100-km atmospheric screening layer for solar Ly β. For zenith observations at Arecibo, solid earth shadow heights of 600 and 1000 km correspond to shadow heights of about 710 and 1120 km, when the screening layer is included.

Similarly, the morning to evening ratios of column abundance for the $[H]_c$ data from satellites D2A and OGO 6 have been calculated and are presented in Table 3 as R_{D2A} and $R_{OGO\,6}$. The calculations were again made for three temperature structures, morning T_c = evening T_c, MSIS T_c values, and measured temperature values. Contrary to the theoretical results of *Tinsley et al.* [1975], *Emerich and Cazes* [1977] found a depletion of $[H]_c$ in the D2A measurements near 0400 LT, as did *Vidal-Madjar and Thomas* [1978] in their analysis of OGO 6 data. This "trough" in $[H]_c$ was especially evident at mid-latitudes.

There is good agreement between R_{NI} and R_{TIN-} for the case of MSIS morning T_c and evening T_c, implying that the model case

TABLE 2. Quadratic Coefficients of Reduced Chi-Square Fit to Normalized Intensities

	Evening			Morning		
Campaign	a_0	a_1	a_2	a_0	a_1	a_2
March 1980	26.35	−11.28	1.28	28.35	−12.67	1.48
Nov. 1983	29.64	−11.92	1.27	28.58	−11.08	1.14
Jan. 1984	41.01	−17.06	1.87	56.33	−25.63	3.02
April 24, 1984	45.16	−21.64	2.72	29.57	−13.26	1.55
April 29, May 5, 1984	35.30	−12.31	0.94	36.59	−12.15	0.88
Nov. 1984	50.73	−21.51	2.39	83.32	−40.49	5.13

TABLE 3. Morning to Evening Hydrogen Column Abundance Ratios

	March 1980	Nov. 1983	Jan. 1984	April 24, 1984	April 29, 1984 May 4, 1984	Nov. 1984
$F_{10.7}$	144	104	86	141	183, 118	79
$F_{10.7}$	188	104	105	128	128	75
$R_{L\beta}$	2.40	1.67	1.61	2.02	2.22	1.39
			600 km [710 km with 100-km screening]			
LT, morning	0458	0449	0512	0420	0416	0453
LT, evening	2015	1932	1946	2029	2032	1931
T_{MSIS}, morning	913	781	724	912	915	679
T_{MSIS}, evening	1121	939	866	1051	1055	802
T_{meas}, morning	1329	942	1186	1320	1076	1407
T_{meas}, evening	930	925	778	944	1025	1129
R_{NI}	0.94	1.05	1.05	0.78	1.15	1.11
			Morning T_e = evening T_e			
$R_{OGO\ 6}$	0.85	0.84	0.86	0.80	0.80	0.84
R_{D2A}	0.77	0.91	0.99	0.63	0.59	0.93
R_{TIN+}	1.65	1.74	1.67	1.64	1.64	1.74
R_{TIN-}	1.26	1.30	1.28	1.24	1.24	1.30
			T_e = MSIS Values			
$R_{OGO\ 6}$	0.66	0.66	0.69	0.67	0.67	0.76
R_{D2A}	0.60	0.73	0.79	0.53	0.50	0.84
R_{TIN+}	1.29	1.38	1.33	1.38	1.38	1.58
R_{TIN-}	0.98	1.03	1.02	1.04	1.04	1.18
			T_e = Measured Values			
$R_{OGO\ 6}$	1.30	0.86	1.42	1.19	0.85	1.08
R_{D2A}	1.18	0.93	1.62	0.94	0.63	1.20
R_{TIN+}	2.52	1.78	2.75	2.44	1.74	2.25
R_{TIN-}	1.92	1.33	2.10	1.84	1.31	1.68
			1000 km [1120 km with 100-km Screening]			
LT, morning	0431	0423	0443	0351	0346	0425
LT, evening	2040	1959	2014	2059	2102	1958
T_{MSIS}, morning	924	784	727	915	918	682
T_{MSIS}, evening	1090	919	848	1024	1025	787
T_{meas}, morning	1379	1111	1039	1003	1011	1100
T_{meas}, evening	730	902	685	944	755	886
R_{NI}	0.91	1.07	0.99	0.79	1.17	1.04
			T_e = Evening			
$R_{OGO\ 6}$	0.82	0.79	0.80	0.92	0.92	0.79
R_{D2A}	0.66	0.71	0.73	0.50	0.51	0.73
R_{TIN+}	1.60	1.69	1.65	1.54	1.54	1.69
R_{TIN-}	1.24	1.27	1.25	1.22	1.20	1.27
			T_e = MSIS Values			
$R_{OGO\ 6}$	0.63	0.60	0.61	0.76	0.77	0.61
R_{D2A}	0.51	0.55	0.56	0.42	0.43	0.57
R_{TIN+}	1.23	1.30	1.26	1.28	1.29	1.31
R_{TIN-}	0.95	0.94	0.96	1.02	1.01	0.98
			T_e = Measured Values			
$R_{OGO\ 6}$	2.21	1.10	1.63	1.01	1.49	2.14
R_{D2A}	1.77	0.99	1.48	0.56	0.84	1.98
R_{TIN+}	4.30	2.36	3.34	1.70	2.50	4.58
R_{TIN-}	3.32	1.72	2.54	1.34	1.95	3.44

of *Tinsley et al.* [1975], with no diurnal winds, zero F_{CE}, and a total upward flux equal to F_J, best matches our measurements. However, the temperatures calculated by MSIS (T_{MSIS}) are much different from those we have measured. While the MSIS model predicts that morning T_e is lower than evening T_e, we have found that the morning temperatures are actually consistently higher than the evening temperatures at similar shadow heights (T_{meas} in Table 3). Using T_{meas} to calculate column abundances from (13), R_{D2A} and $R_{OGO\ 6}$ agree more closely with our measurements (R_{NI}) than do R_{TIN-} or R_{TIN+}. Thus, the temperatures we have measured imply that $[H]_c$ is indeed depleted around 0400–0530 LT, relative to 1930–2030 values. The model of *Tinsley et al.* [1975] was based upon a diurnal temperature structure very similar to that calculated by MSIS, with a minimum around 0400. This appears to be invalid at Arecibo. Since the ratios of morning to evening column abundances that we have measured are nearly equal to unity and the measured temperatures are greater in the morning than in the evening, there apparently exists a persistent depletion in morning $[H]_c$ relative to evening $[H]_c$. This supports the

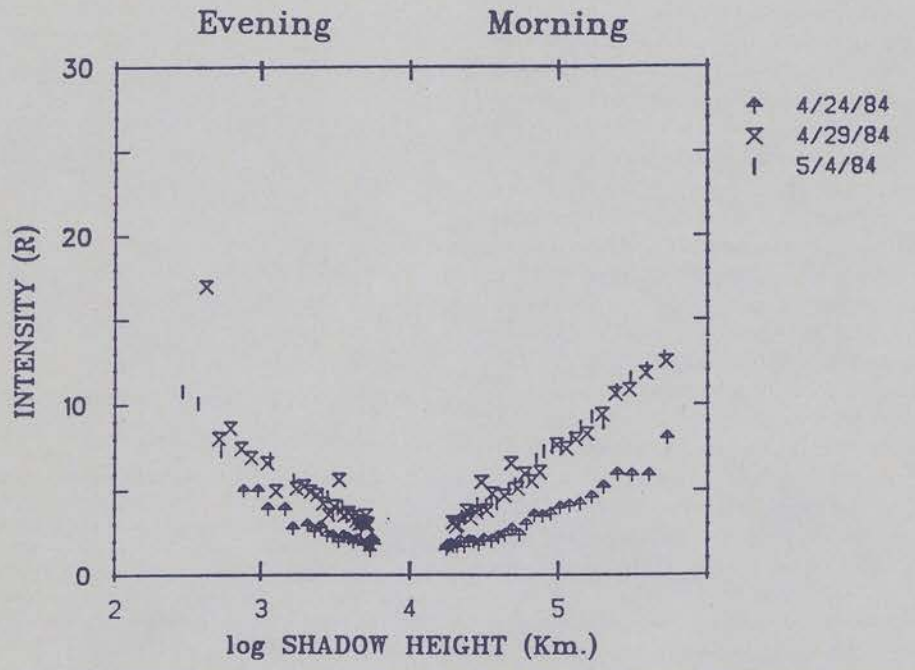

Fig. 6. Scatter plot of the intensities measured during the April–May 1984 period. The absolute intensities have been normalized to solar minimum Ly β flux conditions.

existence of the early morning $[H]_c$ trough, as first described by *Emerich and Cazes* [1977] and *Vidal-Madjar and Thomas* [1978]. The depletion apparently extends to the latitude of Arecibo and is contrary to the smooth sinusoidal variation of $[H]_c$ with local time given by the model of *Tinsley et al.* [1975].

The caveat in concluding that the 0400 trough of $[H]_c$ occurs at Arecibo is the determination of temperature. The measured temperature from an emission column with a base at 710 or 1120 km is certainly not equal to the temperature at the exobase and may be representative of the mean square hydrogen velocity at a much greater altitude, due to the column-integrated nature of our measurements. However, it seems unlikely that the real value of T_c is lower in the morning hours than in the evening, while the effective temperature above 710 km persistantly displays the converse situation.

The only difference between the morning and evening viewing geometries is that the azimuth of the sun relative to the observation direction (zenith) is in a different quadrant. The shadow heights are similar, the solar depression angles are similar, and the relative solar azimuths are equal, but the sun is westward in the evening and eastward in the morning. The extinction of solar Ly β as it passes through a diurnal maximum hydrogen concentration to the east of Arecibo might be adequate to explain the absence of an H_α intensity maximum in the early morning hours (B. Tinsley, personal communication). Furthermore, the absence of an intensity maximum appears to be contrary to the hydrogen densities measured by AE-C in the thermosphere (*Breig et al.*, 1985). Nevertheless, it appears that during our observations the morning hydrogen temperature above the exobase is usually greater than it is in the evening, and that $[H]_c$ near 0400 LT is actually lower than it is around 2000 LT.

Figure 6 shows intensity data, normalized to solar minimum Ly β flux conditions, for the April–May, 1984 period. We find a remarkable increase in the intensities during the morning hours of April 29 and May 5, relative to those measured on April 24. This implies an increase in the column abundance of hydrogen above the morning exobase by a factor of 2 in a period of 5 days. The solar Ly β flux increased only by about 11% from April 24 to April 29, 1984, based on the correlation (9). The markedly enhanced intensities measured only 5 days after April 24, 1984, can be due to some large deposition of hydrogen at Arecibo, or the presence of an additional H excitation mechanism, or large enhancement of the solar EUV flux. A geomagnetic storm

TABLE 4. Column Abundance Enhancement Over March 1980 Values

	710 km				1120 km			
Campaign	R_{TA}	R_{VM}	R_J	R_{NI}	R_{TA}	R_{VM}	R_J	R_{NI}
				Evening				
Nov. 1983	1.50	1.70	2.60	1.29	1.39	1.58	2.42	1.32
Jan. 1984	1.80	2.20	4.32	1.66	1.61	1.96	3.93	1.67
Nov. 1984	2.15	2.81	7.36	1.93	1.84	2.41	6.45	1.93
				Morning				
Nov. 1983	1.43	1.65	2.90	1.45	1.35	1.57	2.82	1.54
Jan. 1984	1.69	2.11	5.24	1.85	1.54	1.94	4.89	1.81
Nov. 1984	1.94	2.61	9.03	2.29	1.71	2.31	8.10	2.20

began on April 25 and reached major storm levels on April 26. These levels persisted throughout the night of April 29, when the field was intermittently active. Also, a proton precipitation event began on April 25, peaked on April 26, and persisted through April 29. Several injections were reported during the period. H_α line profiles from April 29 showed no evidence of a secondary excitation mechanism. It seems plausible that a significant, impulsive enhancement of exospheric hydrogen abundance occurred at Arecibo after April 24, 1984, which was associated with the geomagnetic storm period. Such an event illustrates that dramatic changes in exospheric hydrogen abundance can occur within time periods on the order of days and that solar cycle variations inferred from a small number of data points along the solar cycle must be interpreted with care.

Solar cycle variation. Referring to Figure 5 and Table 4, the expected pattern of increasing hydrogen abundance with decreasing solar activity is evident. The lowest abundances are measured during the period of highest solar activity (March 1980), while the greatest abundances are found during the solar minimum conditions of November 1984. Table 3 lists the relevant values of the $F_{10.7}$-cm flux.

Table 4 shows the hydrogen column abundance enhancement factors relative to the abundance measured in March 1980. In this table, R_{TA} is the enhancement predicted using (13) and (14) and the coefficients of *Thomas and Anderson* [1976]. R_{VM} in Table 4 is the enhancement factor over the March 1980 period, using the coefficients for (12) calculated by *Vidal-Madjar* [1978]. R_J is the enhancement factor based on a pure thermal escape calculation, and R_{NI} is the enhancement implied by our measurements, which have been adjusted for the variation in the solar Ly β flux. We measure a factor of 1.93 increase in the column abundance of exospheric hydrogen between the conditions of March 1980 and the low solar activity conditions of November 1984. The ratio R_{NI} was determined using low shadow height data, so that the effects of multiple scattering are expected to be small.

As many earlier investigations have shown, the increase of hydrogen abundance with decreasing solar activity is much smaller than predicted by assuming that the abundance is modulated solely by thermal escape. Our results are in reasonable agreement with the empirical formulations of *Thomas and Anderson* [1976] and *Vidal-Madjar* [1978]. There appears to be a slight underestimate of the hydrogen abundance for solar minimum conditions using the values reported by Thomas and Anderson, as suggested by *Vidal-Madjar* [1978]. On the other hand, the formulation of Vidal-Madjar appears to slightly overestimate the abundance during solar minimum conditions. These conclusions depend upon the validity of using (13) to determine column abundances from the empirical formulation of $[H]_c$ (equation (11)), and upon variations in the local exobase conditions during our observing periods. In any event, our ground-based results do not deviate substantially from earlier observations of geocoronal hydrogen abundance, from which (11) has been determined [*Vidal-Madjar*, 1978].

7.2 *Exospheric Temperature*

In Figure 7 the variation of H_α line width with local time and viewing geometry is shown for the March 1980 period. The solar activity during the observations was moderate, but the 81-day average solar flux was more characteristic of high solar activity conditions (Table 3). A notable feature in Figure 7 is the large decrease in effective temperature near solar midnight, which occurs at 0024 LT. This minimum is presumably due to gravitational cooling at a large geocentric distance, although it may also be due to a satellite particle population with small orbital eccentricities. It is also evident that the line widths measured in the morning hours are broader than those measured at similar shadow heights in the evening hours. The higher temperature near the morning exobase relative to the evening exobase is not in agreement with the MSIS values, which slowly decrease from evening to morning.

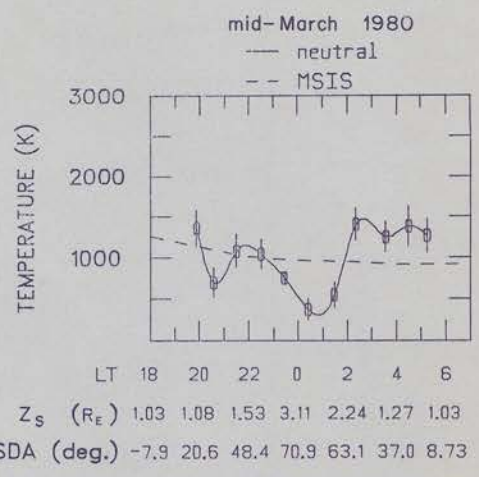

Fig. 7. The nighttime variation of effective hydrogen temperature in March 1980 versus local time; the shadow height, using 100 km screening (Z_S); and the solar depression angle (SDA). The solid line is a cubic spline fit to the data, which is represented with two standard deviation error bars. Values of the exobase temperature calculated by the MSIS model [Hedin, 1983] are shown by the dashed line. The data has been summed at similar local times on March 14 and 18, 1980, prior to the temperature analysis.

Figure 8 shows the variation in effective temperature for 3 nights in the spring of 1984. The midnight decrease in effective temperature is less apparent in these results than in Figure 7. This could be due to the fact that the midnight observations in Figure 8 correspond to smaller geocentric distances. There does appear to be some decrease near solar midnight in Figures 8*b* and 8*c*, but the minimum is displaced toward 0200 on April 24, 1984 (Figure 8*a*). In general, there is good agreement between the MSIS results and our measurements. However, the temperatures measured above the morning exobase are again greater than above the evening exobase, although this effect is less pronounced than it was in March 1980.

The nighttime variability of the line widths is slightly greater on May 4, 1984, than on either April 24 or April 29, 1984 (Figure 8). The results shown in Figures 9*a* and 9*b* also display a very large variability. The greatest variability of line width occurs for low solar activity periods, while data for moderate to high periods of solar activity tend to exhibit much smaller variability in line widths. One possible explanation for this tendency is that charge exchange proceeds more efficiently during the periods of low solar activity, and the mean square velocity of the neutral hydrogen population is therefore more dependent upon the state of the exospheric plasma during these times. The smallest nighttime variation of line widths for the April–May 1984 period occurred when the $F_{10.7}$-cm flux reached a value of 183 on April 29 (Figure 8*b*). A slightly larger variability is evident for April 24, when the $F_{10.7}$-cm flux was 141, and the greatest variability is seen in the data from this period when $F_{10.7}$ dropped to 118 on May 4.

There is not only a great variability in the effective tempera-

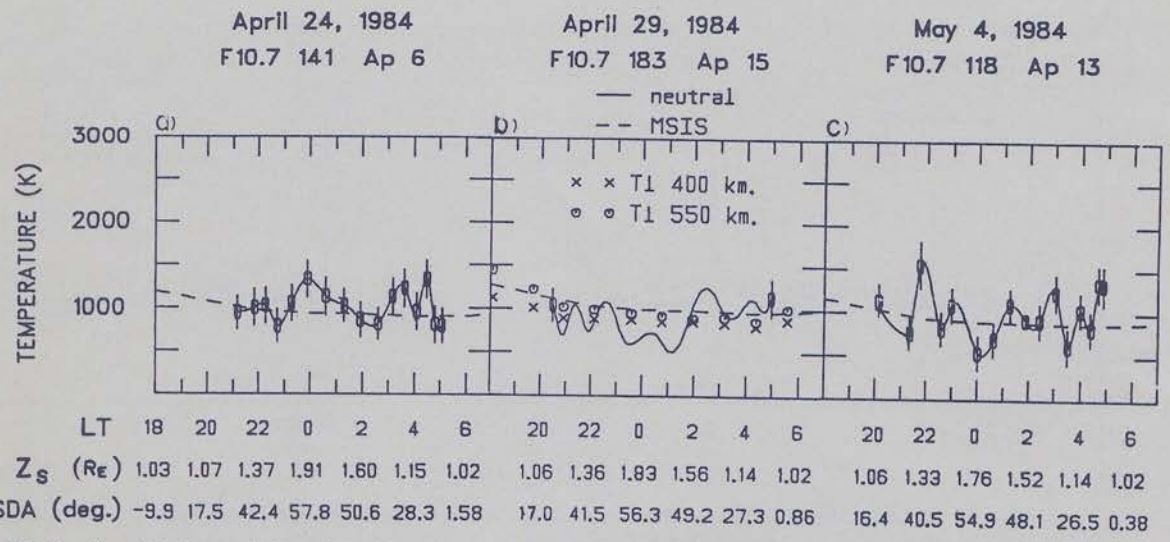

Fig. 8. The nighttime variation of the effective hydrogen temperature for three dates during the spring of 1984. The symbols are the same as described in Fig. 7. Ion temperatures are shown for April 29, 1984. For clarity, only the first and last hydrogen temperature data points are shown in Figure 8*b*. Ion temperature errors are about 20 K below 500 km, increasing to 25% above 600 km.

tures measured in November 1983 and January 1984, but the temperatures also appear to be surprisingly high. Only during the twilight periods, when the shadow heights are near to the assumed exobase altitude of about 500 km, is there reasonable agreement with the MSIS values (Figure 9). As the base of the emission column increases to altitudes above about 1.5 R_e, the line widths become very broad, and there is little evidence of a midnight minimum. To avoid galactic contamination, observations were made at a zenith angle of 15° between 2118 and 0040 LT in January 1984. Nevertheless, the line widths measured in the zenith near 0100 LT, corresponding to a shadow height of about 6 R_E, are not nearly as narrow as might be expected on the basis of gravitational cooling.

The reason for the high effective temperatures measured in November 1983 and January 1984 appears to be related to efficient charge exchange above the exobase during these periods, coupled with the column-integrated nature of our data. Not only was solar activity low in November 1983 and January 1984, but the measured ion temperatures increased more rapidly with altitude than was the case in April and May 1984. This is shown in Figures 8*b*, 9*a*, 9*b*, and 10. Furthermore, the vertical ion velocities measured at Arecibo in the winter are often strongly negative (downward), suggesting that the flow of hot neutral hydrogen following charge exchange will be downward (Figure 11). This enhances the mean square neutral hydrogen velocity and heats the ballistic component. Figure 11*c* shows that the vertical ion velocities were not strongly downward in the spring of 1984, when our measured neutral line widths were not nearly so broad. Although the vertical velocities shown in Figure 11 are for altitudes near the exobase, there is an indication that the wintertime velocities become more strongly negative with altitude. There have been other reports of negative

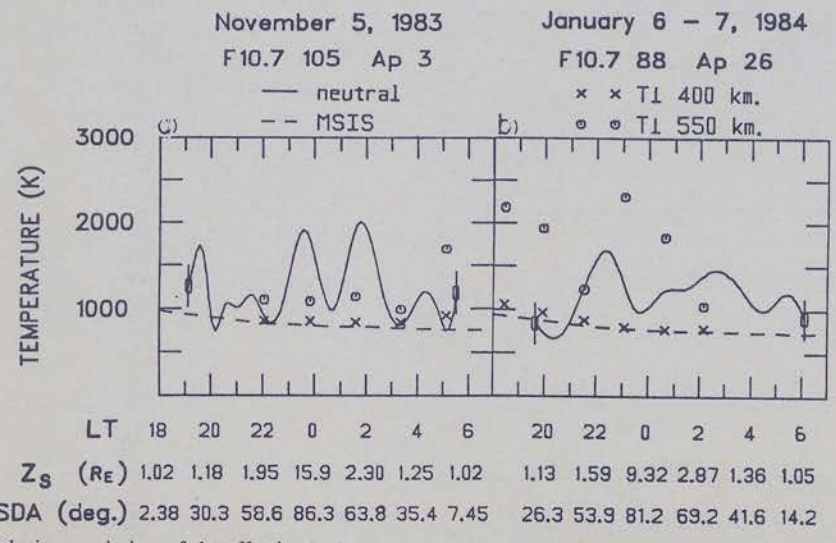

Fig. 9. The nighttime variation of the effective hydrogen temperature in November 1983 and January 1984 and the ion temperature at two altitudes. Only the first and last hydrogen temperature data points are shown. Symbols are the same as for Fig. 7. The data for Figure 9*b* have been summed at similar local times on January 6 and 7, 1984, prior to neutral temperature analysis.

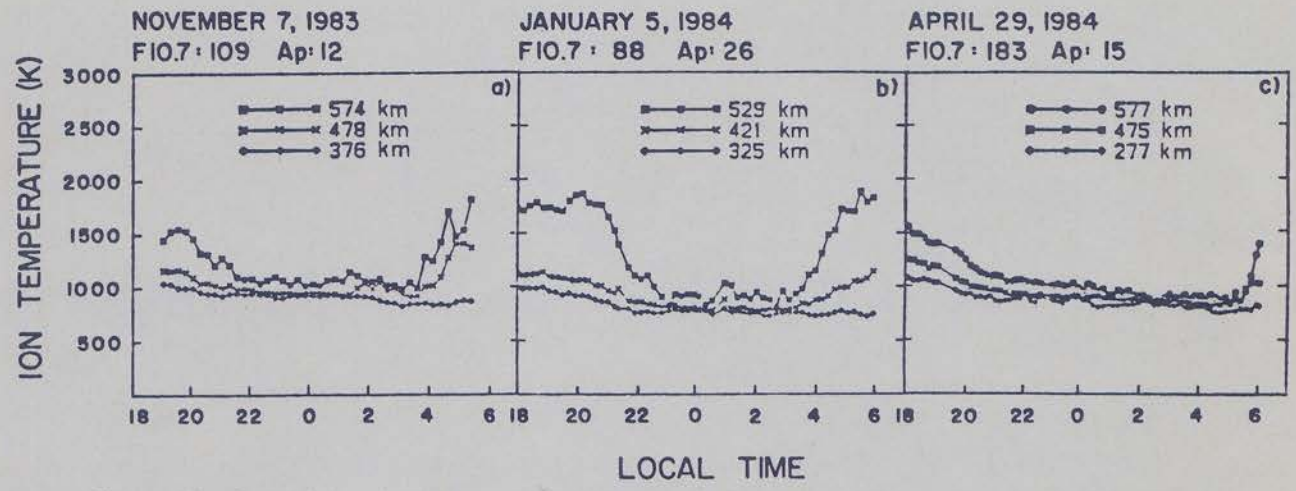

Fig. 10. Nighttime variation of the ion temperature at three altitudes for three observing periods corresponding to Figures 8 and 9. Errors in the ion temperatures are described in Fig. 8.

ion velocities in the *F* region during the winter at Arecibo [*Vickrey et al.*, 1979; *Burnside et al.*, 1985] and indications that the vertical velocity becomes more negative with altitude. It therefore seems reasonable to assume that there is a persistent downward flux of hot protons in winter at Arecibo, even for altitudes well above the exobase.

Differences between H^+ and O^+ velocities have been detected at Arecibo by *Vickrey et al.* [1979]. Their results indicated that H^+ generally flows more strongly downward than O^+ and that H^+ may actually flow slightly downward when O^+ is moving upward. The reason for this is that the diffusion coefficient for H^+ is larger than that for O^+. The work of *Vickrey et al.* [1979] also showed that the base of the protonosphere, defined as the altitude at which the concentration of H^+ equals that of O^+, falls dramatically after sunset from 1170 km to about 550 km during nighttime hours.

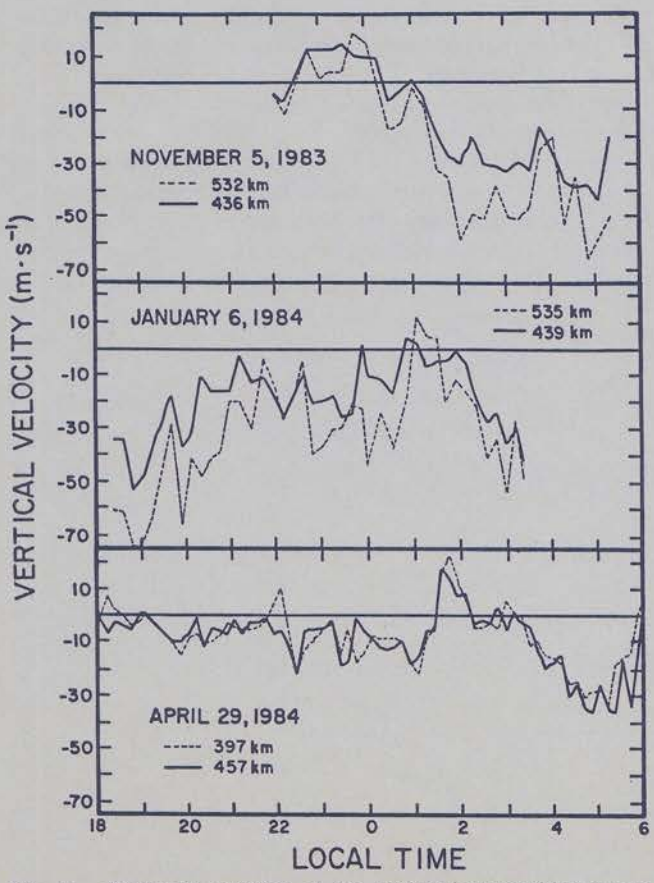

Fig. 11. Nighttime variation of the vertical ion velocities at two altitudes corresponding to the three observation periods of Figures 8, 9, and 10. The radar chirp offset has been accounted for in all cases, and the uncertainty is roughly ±10 m s^{-1}. Velocities are positive upward.

We therefore feel that there is much to support the assertion that there is an enhancement in neutral hydrogen temperature above the morning exobase at Arecibo and that it is due to charge exchange, especially during the winter months. Figure 11 shows that the largest downward ion speeds are often observed between about 0200 and 0600 LT. The largest negative velocities measured in April 1984 occurred between 0400 and 0600 LT.

Our radar data awaits compositional analysis, but earlier studies indicate that the H^+/O^+ ratio maximizes in the early morning hours (Table 5) [*Bailey et al.*, 1982; *Ho and Moorcraft*, 1975]. *Maher and Tinsley* [1978] present $[H^+]$ data from Arecibo at 1050 km that show a diurnal maximum in the morning hours as well. A diurnal maximum of $[H^+]$, combined with vertical ion velocities that are strongly downward, results in a downward flux of H^+ in the morning hours that contributes to an energetic, ballistic, neutral H component via charge exchange. The resultant H_α line profile we measure is broadened as a result of

TABLE 5. Nighttime Percent Ion Concentration Above the Exobase at Arecibo

Time, AST	560 km			630 km		
	O^+	He^+	H^+	O^+	He^+	H^+
1800	92	0	8	90	0	10
2000	90	0	10	87	0	13
2200	85	2	13	77	1	22
0000	80	3	17	71	2	27
0200	66	3	31	50	5	45
0400	61	8	31	26	30	44
0600	73	5	22	58	22	20
0800	89	0	11	79	0	21

Data from *Ho and Moorcraft* [1975].

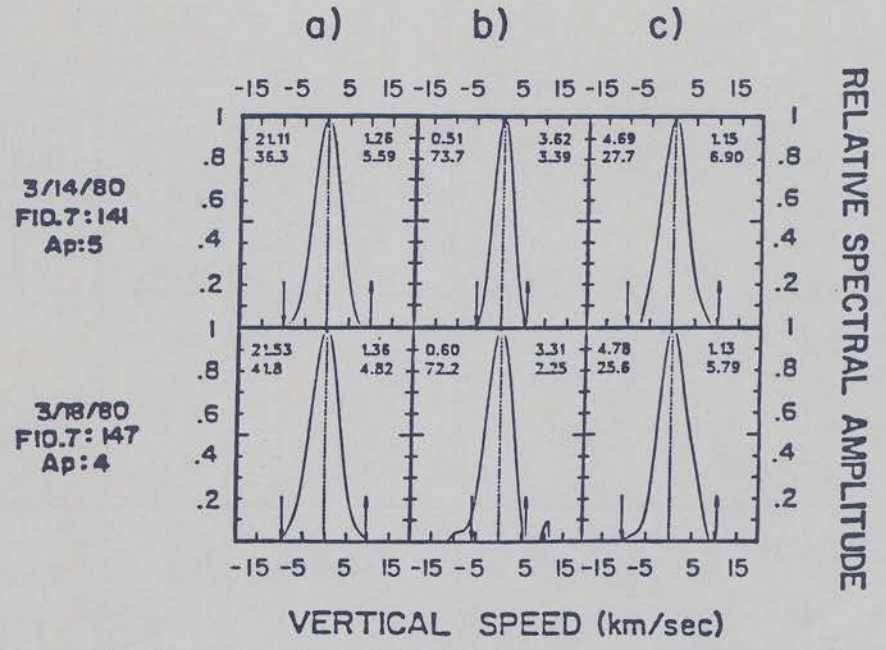

Fig. 12. A representative collection of pure, deconvolved H_α emission profiles obtained in March 1980. Each profile has been normalized to the intensity at line center. Negative velocities are downward. To the upper left of each profile the local time is printed in decimal hours, and the number below that is the solar depression angle. The lower value to the right of the profile is the λ value, which is defined as the ratio of the squares of the escape velocity (equation (7)) and the most likely Maxwellian velocity (equation (3)). The upward arrows define the escape velocity appropriate for the altitude of the shadow height, which is defined in terms of earth radii to the upper right of each profile. A screening altitude of 100 km is used. The downward arrow is merely the reflection of the upward escape velocity arrow and is included to assist visual inspection of symmetry. For each date the profiles go from evening (Figure 12*a*, to solar midnight (Figure 12*b*) to morning (Figure 12*c*).

the enhanced mean square velocity of the hydrogen population. Although strongly downward ion velocities are sometimes measured in the evening hours (Figure 11*b*), the flux of protons is probably not as great as during the morning hours, because of the lower H^+ density in the evening (Table 5).

It is possible that the early morning depletions of $[H]_c$ measured by spacecraft D2A in April 1971 [*Emerich and Cazes*, 1977] and OGO 6 near the 1969 fall equinox [*Vidal-Madjar and Thomas*, 1978], may be related to the loss of hydrogen due indirectly to charge exchange. Although the preferred direction of the hot neutral hydrogen created is downward during the morning hours, the upward "splash" escape flux of reflected hot neutrals discussed by *Chamberlain* [1977] may be significant during these periods. Also, subsequent collisions of the energetic, downbound H with exospheric H will cause secondary heating that can enhance the escape flux. Such conclusions are speculative, however, and *Tinsley et al.* [1975] have calculated that F_{CE} reaches a diurnal minimum in the early morning hours.

7.3 *Evaporative Cooling*

The cooling of neutral hydrogen relative to oxygen near the exobase due to the escape of hot, energetic hydrogen has been difficult to detect in our data. This effect is expected to be most evident for high solar activity conditions, and we have no simultaneous optical and radar data for high solar activity. Furthermore, the line profiles we measure may be broadened by contributions from a hot hydrogen component at higher altitudes than the base of the emission column, due to charge exchange with hot protons well above the exobase.

There is some indication that the neutral hydrogen temperature near the exobase (where the velocity distribution is still Maxwellian) on April 29, 1984, is slightly less than the temperature of O^+ in the topside F region (Figure 8b, evening). There is no evidence of the cooling in any of our measurements near the morning exobase, and the possible cooling seen in the evening hours of April 29, 1984, is not beyond the limits of the error bars.

7.4 *Line Profiles*

Figures 12 through 15 show pure, deconvolved, H_α source profiles from our four observing campaigns since March 1980. These line profiles may be interpreted as exospheric radial velocity distributions of atomic hydrogen.

Figure 12 shows line profiles obtained from the zenith in March 1980. Except for the profile from near solar midnight on March 18 the profiles contain very few particles with velocities greater than the escape velocity at the altitude corresponding to the base of the emission cone. The low shadow height profiles are essentially Gaussian, illustrating that the velocity distribution is nearly Maxwellian at these altitudes. The profiles near midnight are narrow, presumably due to gravitational cooling at distances of about 3.5 R_E. There is some indication of a depleted blue side relative to the red in the morning hours, suggesting a smaller population of energetic inbound hydrogen compared to the outbound population. There is evidence of a small, hot inbound component in the midnight profile of March 18, perhaps due to charge exchange at great altitude, and there is some indication of a very slight outbound component of similar energy. The sharp cutoff of the outbound high-energy component may be an artifact of the deconvolution procedure.

Figure 13 shows line profiles from four dates in November 1983. These have much more structure than those observed in March 1980. There is generally good reproduction of certain features seen for similar viewing geometries. Figure 13 *a* shows a

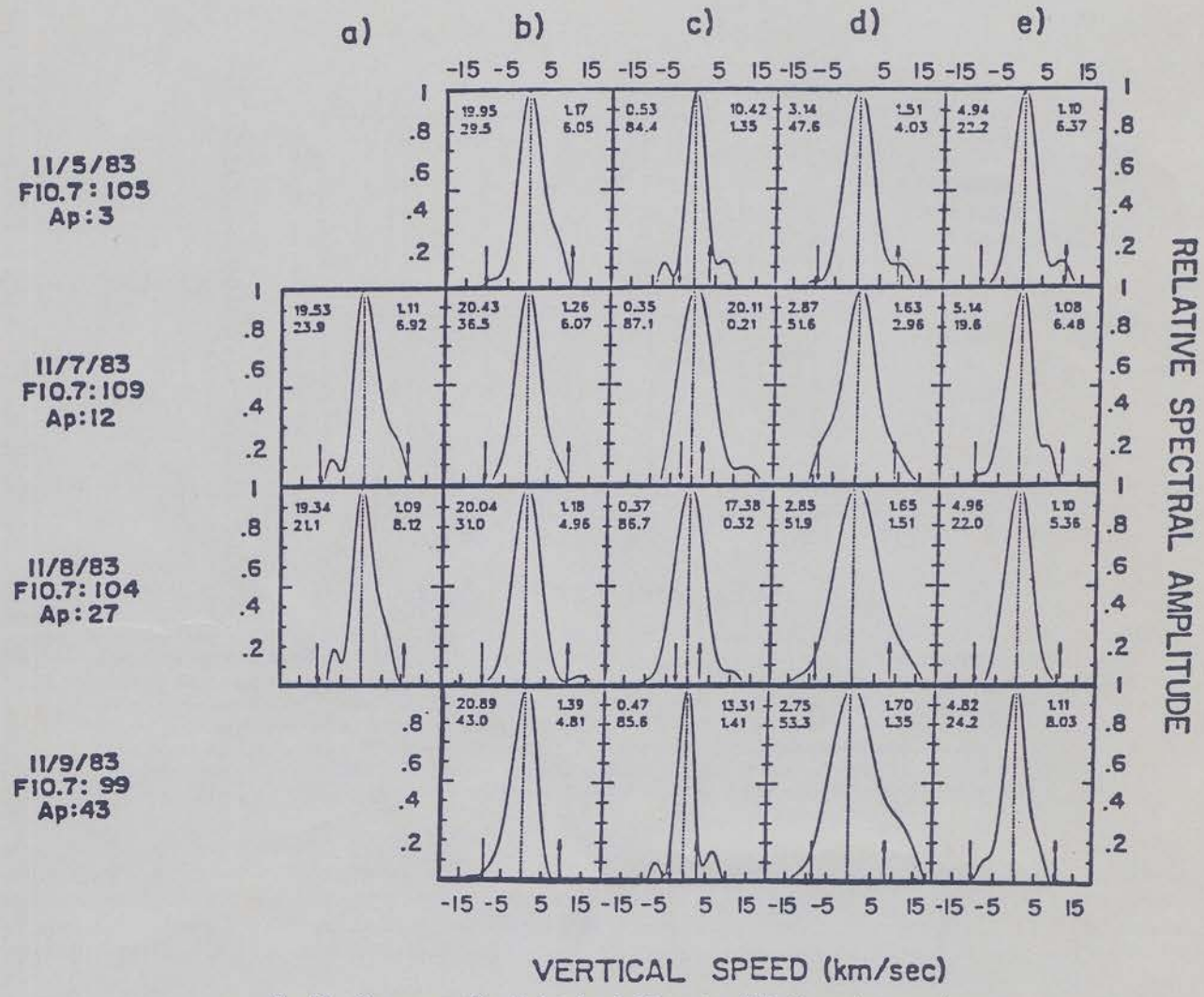

Fig. 13. The same as Fig. 12, but for the November 1983 observation campaign.

bump at about -7 km s^{-1} and some red side shouldering on both November 7 and 8. There is also a pronounced broadening of the profiles near 0300 LT on each night (Figure 13*d*). The degree of broadening appears to correlate well with increases in geomagnetic activity. These broad profiles are also coincident with the strong downward ion velocities measured on November 5 (Figure 11*a*). This seems to support the idea that charge exchange may be causing a significant enhancement of neutral hydrogen velocities during this period. The wings of the profiles in Figure 13*d* are the most enhanced on the outbound side, but there is significant enhancement of the inbound side as well.

For most of the profiles in Figure 13 the incoming side is slightly narrower at the half height, especially near the evening exobase (Figure 13*a*). This effect is somewhat diminished near 1.20 R_E (1300 km) but is still evident on November 11 (Figure 13*b*). Near the morning exobase (Figure 13*e*) there is actually an enhancement of the line width on the incoming side compared to the outgoing side, which is most evident on November 11. By calculating the areas beneath the profiles we measure a slight enhancement of the inbound hydrogen population near the morning exobase (Figure 13*e*) for each of the dates, with the exception of November 9.

The profiles from near solar midnight in November 1983 represent the highest shadow height data that has been obtained. On November 5 and 9 there appears to be narrowing of the profiles due to gravitational cooling out to about 13 R_E. The midnight profiles of November 7 and 8 correspond to shadow heights of nearly 20 R_E. For these very great shadow heights the profiles become much broader than would be expected from the limits of gravitational cooling. During these periods it is possible that the profiles are strongly affected by multiple scattering of solar Ly β into the shadow cone at much lower altitudes.

The narrow profiles with shouldered wings that occur inside the value of the escape velocity are possibly due to a satellite particle population. It is possible that satellite populations could be responsible in part for the profiles shown in Figure 13*e*, for November 5, 7, and 9. The same may also be said of Figure 13*a*.

The December and January profiles in Figure 14 are similar to those of Figure 13, but with even greater distortions. In general, the profiles obtained in December 1983 and January 1984 show very significant enhancements in the wings. There is a significant contribution to the measured emission near +10 km s^{-1} near solar midnight on each night (Figure 14*b*). This bulge is most evident for observations with shadow heights near 6 R_E. There is very little narrowing of the profile widths at large shadow heights, when compared to the twilight profiles.

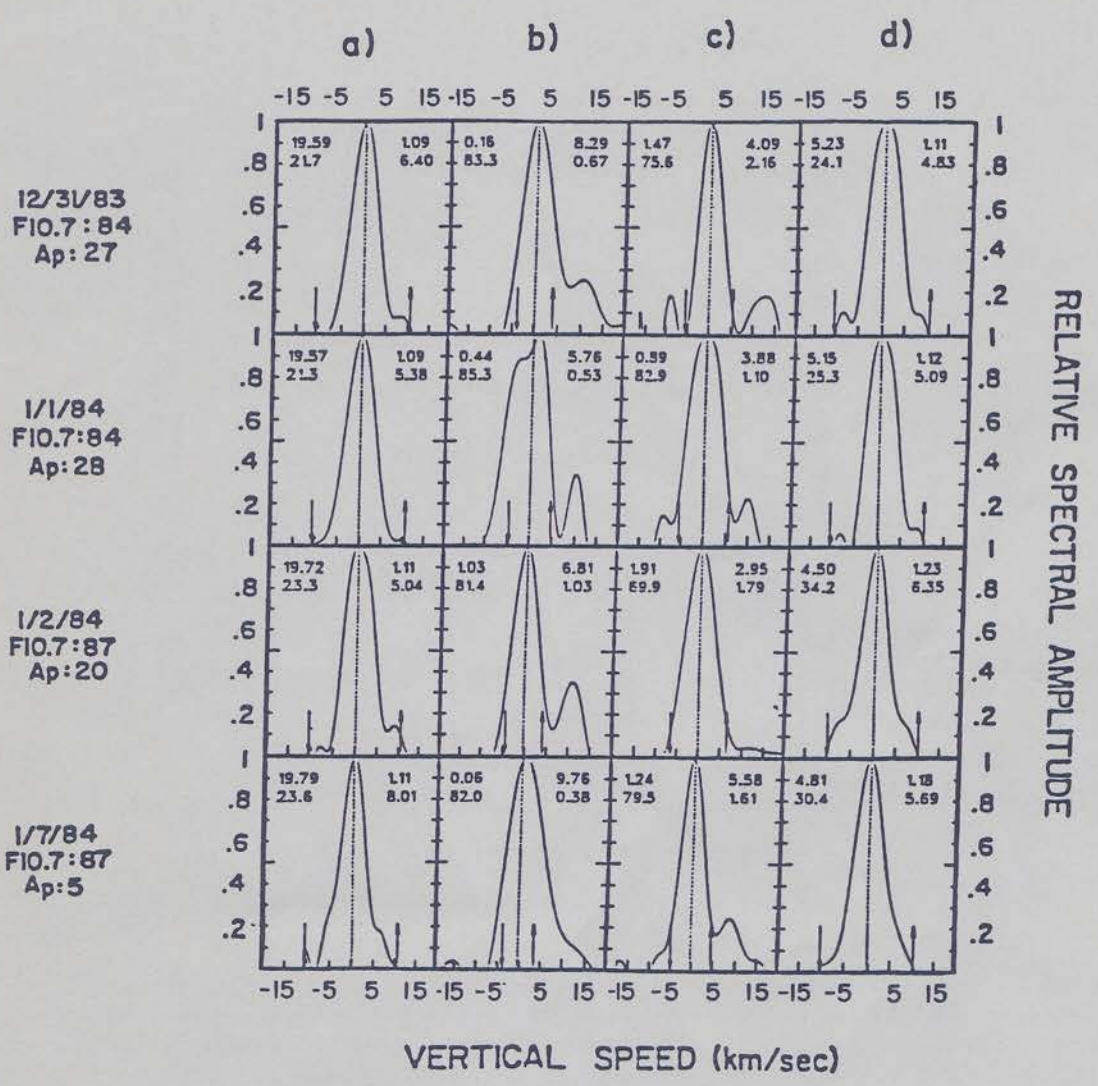

Fig. 14. The same as Fig. 12, but for the December 1983, through January, 1984 period.

It has been suggested that collisional excitation of the Balmer alpha fine-structure emission lines not present in Ly β excitation [*Yelle and Roesler*, 1984, 1985] may cause asymmetries, especially on the red side of the $3^2P_{3/2}$, $3^2P_{1/2} - 2^2S_{1/2}$ conjugate H_α resonance line (see appendix). None of the other fine-structure lines occur at the location of the bulge seen in Figures 14*a* and 14*b*. We believe that the distortions seen in Figure 14 are primarily due to a neutral hydrogen velocity distribution above the exobase that is greatly perturbed by charge exchange in the protonosphere. In many profiles, emission features in the inbound wing correspond exactly in velocity to outbound wing distortions. These features are clearly not due to emissions from other fine structure H_α components, since there is no fine-structure line to the blue of -0.7 km s^{-1} from the conjugate geocoronal H_α line center (see appendix).

Interhemispheric flow of protons from the summer to winter hemispheres (thermal energies <1 eV) can supply the downward flux of protons observed at Arecibo in the winter [*Vickrey et al.*, 1979; *Bailey* et al., 1982]. A source of higher-energy protons (>10 eV) that may cause collisional excitation of H_α at Arecibo is not available.

The profiles obtained in the morning twilight in December 1983 and January 1984 (Figure 14*d*) may be indicative of a significant satellite particle population. There does appear to be some peaking near line center. However, this is indistinguishable from a cool neutral hydrogen population that also contains some filling in of the line wings due to the creation of energetic neutrals by charge exchange. While it is generally possible to exclude satellites as being responsible for shouldering which occurs beyond the limit of the escape velocity at a given altitude, it is not possible to attribute shouldering which occurs within that limit unambiguously to a satellite particle population. Nevertheless, the shouldering evident in Figure 14*d* is so symmetric that it suggests a peaking at line center due to contributions from a satellite population with small orbital eccentricities being added to an otherwise Maxwellian profile near the exobase. The satellites may contribute to the profiles at these altitudes because the profiles are column integrations.

Line profiles from April and May 1984 are shown in Figure 15. The line shapes measured during this period are rather symmetric, with few wing distortions. The narrowing with increasing altitude is present, and the red side depletion relative to the energetic blue side is often evident. The distortions that are present are much less pronounced than those of Figures 13 and 14. Profiles near the morning exobase (Figure 15*c*), are slightly broader than those near the evening exobase (Figure

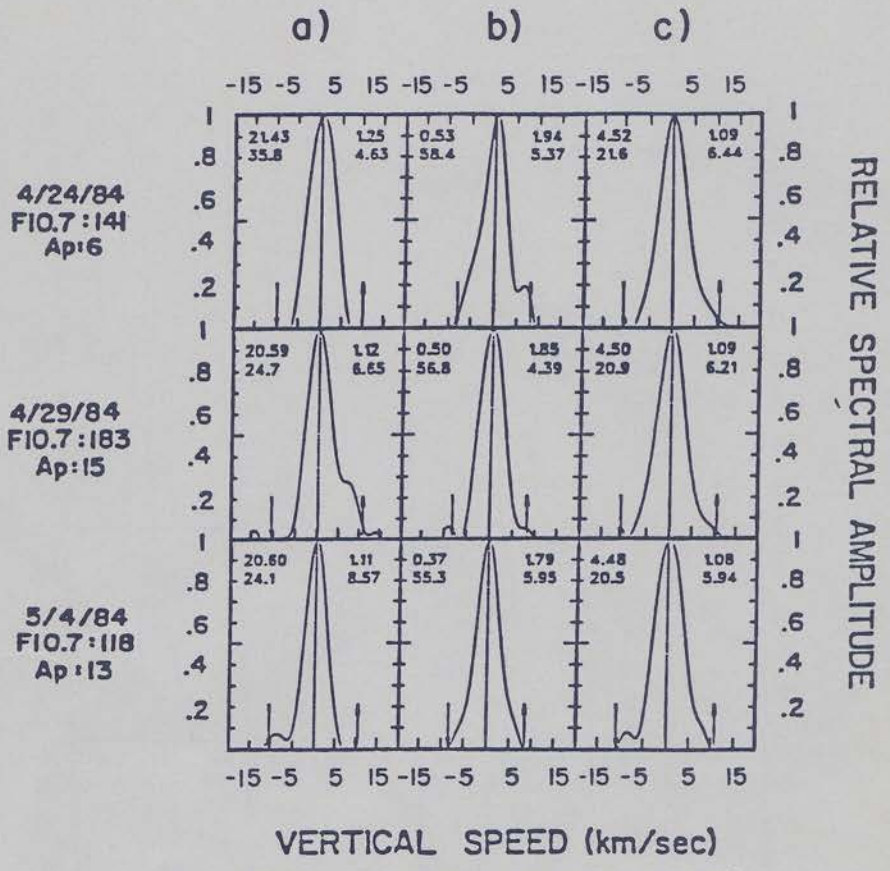

Fig. 15. The same as Fig. 12, but for the April–May 1984 period.

15*a*). The profiles from April 24 (Figures 15*a* and 15*b*) may indicate a satellite population. Vertical ion velocities from this time period were very small (Figure 11*c*). There is slightly greater distortion of the profiles in April and May 1984 than in March, 1980. This may not be too surprising, however, since the hydrogen abundance in March 1980 was lower than it was in April 1984, and charge exchange was likely to have been more important during the solar cycle epoch of spring 1984 than the spring of 1980.

7.5 *Multiple scattering*

The scattering of solar Ly β photons into the region below the shadow height of observation can be detected in the line profile analysis. The nature of the profile contamination due to multiply scattered Ly β depends upon the altitude of stimulated emission and upon its strength relative to that of the directly illuminated emission above the shadow line. It has been suggested that emissions excited well below the exobase by multiple scattering in the mesosphere and lower thermosphere (200 K) may be a large part of the total emission observed for large shadow height observations (J. Bertaux, personal communication, 1985). This contamination would have a characteristically narrow FWHM. On the other hand, emission of H_α due to multiple scattering near 500 km can contaminate profiles from several earth radii in the opposite way, since the neutral temperature at 500 km would give a broad contribution. Emissions from below and near the exobase are expected to be highly symmetric.

Very narrow high shadow height profiles are common. Examples occur in Figures 12*b*, 13*c*, 14*c*, and 15*b*. However, these widths are still characteristic of mean hydrogen temperature hundreds of degrees greater than that of the mesosphere and lower thermosphere. Furthermore, the narrowing of profiles with altitude appears to be primarily related to the inverse relationship between geocentric distance and the escape energy. The profiles are usually contained just within the escape velocity limit for all shadow heights. This would be an unlikely coincidence if the narrow profiles were the result of emission from a source below the illuminated region.

The occasions when the H_α line profiles show large H populations exceeding the energy required for escape (Figures 13*c*, 13*d*, 14*b*, and 14*c*) may be due to hot emissions from near the exobase excited by multiple scattering. These emissions should be mostly symmetric, however, and it is difficult to explain most of the profile wing distortions with a multiple-scattering source. Figure 13*c* shows the highest shadow heights for which we have obtained data. The profiles in Figure 13 appear to narrow in a manner to be expected by the escape energy constraint until about 13 R_E. Broad, symmetric profiles were observed for shadow heights above 17 R_E on November 7 and 8, 1983 (Figure 13*c*). These profiles extend well beyond the escape speed. A similar departure from the narrowing due to gravitational cooling seems to occur near 6 R_E in January 1984 (Figures 14*b and 14c*). It is possible that the broad, mostly symmetric profiles measured above 17 R_E in Figure 13*c* and above 6 R_E in Figure 14*b* may be due to hydrogen emission excited by multiply scattered photons near the exobase.

We believe the broad profiles in Figure 13*d* and the wing distortions evident in Figures 13 and 14 are due primarily to perturbations of the neutral hydrogen velocity distribution by

charge exchange. The greater population of outgoing energetic hydrogen relative to the incoming population evident for observations near 1.6 R_E shadow heights in November 1983 (Figure 13*d*) is contrary to what would be expected from a hot Maxwellian emission source near the exobase.

The line profile data indicate that multiple scattering does not appear to significantly contaminate emissions from the illuminated region for shadow heights below about 5 R_E. We have arrived at a similar conclusion from our H_α intensity data.

Ignoring the background contributions of the zodiacal light, the gengenschein, the diffuse galactic emission, and tropospheric scattering, the entire midnight emission above the interplanetary background of about 0.1 R [*Atreya*, 1973] might be attributed to H_α emission from solar Ly β multiple scattering. This background intensity amounts to about 1–4 R (Figure 5). By determining the level at which the change of intensity with altitude falls to zero and the emission intensity falls to the background level, a conservative estimate of when multiple scattering may be a significant H_α excitation mechanism can be made. For each of the curves in Figure 5 the derivative of intensity with respect to altitude goes to zero when the shadow height exceeds about 10,000 km (2.6 R_E). The intensity falls to background levels for the curves in Figure 5 above $5.3^{+3.9}_{-2.1}$ R_E on the average. The uncertainty represents one standard deviation of the observed values. It appears that H_α emission due to multiply scattered Ly β excitation can be neglected below about 2.6 R_E in our observations and is probably insignificant for observations below 5 R_E.

8. CONCLUSIONS

High-resolution measurements of the geocoronal H_α emission at Arecibo are yielding a wealth of information about the nature of the exospheric hydrogen distribution. The observations presented here display many of the characteristics predicted by current exospheric theory, but the interpretation of certain aspects remains a challenge for future modeling efforts. Conclusions regarding the mechanisms which contribute to observed H_α line shapes and their nighttime, seasonal, and solar cycle variations are necessarily speculative because the data base is still very small. However, the following trends seem to be emerging.

1. H_α line profiles for vertical observations with shadow heights near 500 km are usually representative of a Maxwellian velocity distribution. As the base of the emission column moves upward, H_α line shapes generally display asymmetry between the incoming and outgoing hydrogen populations. Populations of energetic hydrogen with outgoing speeds in excess of the escape speed are greater than incoming populations with similar energies. This general case is sometimes reversed in the morning hours, when the population of incoming hydrogen actually exceeds the outgoing population.

2. An increase in the early morning (0200–0600 LT) effective hydrogen temperature is a persistent feature in our data. These enhanced temperatures are correlated with the diurnal maximum proton concentration above the exobase and often with large downward ion velocities. It appears that a downward flux of hot protons in the early morning hours at Arecibo, which is largest during the winter months, heats the neutral H population by charge exchange.

3. The nighttime variation of the H_α intensity in the zenith is very symmetric about solar midnight, and the ratio of morning to evening intensities measured at similar shadow heights is near unity. Thus the hydrogen column abundance above 700 km in the morning appears to be nearly equal to the abundance above the same altitude in the evening. This implies that the density at 500 km is lower in the morning than in the evening, since the morning temperature and hydrogen scale height appear to be larger than in the evening. It seems that the early morning trough in $[H]_c$ detected by satellites D2A and OGO 6 extends to the latitude of Arecibo, at least for late fall through spring observing periods.

4. Large distortions of H_α radial line profiles have been observed throughout the night during winter observing periods. These observations were also made during low solar activity conditions. The broad spectral widths and prominant wing distortions appear to be correlated with large downward ion velocities and a corresponding downward proton flux above the exobase which occurred throughout the night during our late fall and winter observations. Similar H_α profile distortions were not evident in April and May 1984, when the vertical ion velocities were nearly zero all night. The distortions were not evident in March 1980, when solar activity was at moderate to high levels. We believe distorted H_α line profiles may be common for winter observations near solar minimum, due to charge exchange perturbation of the neutral H_α velocity distribution.

5. Narrow H_α spectral line widths are often measured near solar midnight, when the shadow height in the zenith reaches several earth radii. A procedure which isolates the pure emission source function from the instrument function has been useful in determining that this narrowing is due primarily to gravitational cooling. The required escape energy diminishes with increasing geocentric distance. This results in radial H_α profiles that become increasingly narrow with geocentric distance, due to the escape of lower-energy hydrogen atoms. This effect is most evident during moderate to high solar activity conditions and during the springtime, when the profiles are less perturbed by charge exchange.

6. Our data support the generally held view that multiple scattering of solar Ly β into the shadow region beneath the illuminated column becomes significant only for observations near the antisolar direction. Even for low solar activity conditions, when multiple scattering is expected to be most efficient, line profile evidence indicates that the H_α emission remains characteristic of the directly illuminated region above the shadow height to about 5 R_E. Our intensity data indicates that multiple scattering probably contributes a negligible amount to observed emissions with shadow heights below 3 R_E.

7. We have searched for evidence of a satellite particle population in the H_α source profiles. There is some indication of profile narrowing and shouldering (within the limit of the escape velocity) that resembles the theoretical profiles of *Prisco and Chamberlain* [1979], which were generated for varying populations of satellite particles. These structural similarities must occur for hydrogen in the velocity regime below that required for escape because satellite particles are gravitationally bound. It is not possible to attribute the very narrow profiles obtained near solar midnight to a population of low-eccentricity satellites, since the widths of these profiles are not narrower than would be expected from simple gravitational cooling of geocoronal hydrogen.

8. Cooling of hydrogen near the exobase relative to the topside F region O^+ temperature has not been evident in our data taken during low to moderate solar activity conditions. It is

possible this effect has not been observed because the profiles from which we derive H temperatures are column integrations along the vertical line of sight. Neutral H temperatures observed at shadow heights near the evening exobase were roughly equivalent to the O^+ temperature in the topside ionosphere. The neutral temperature near 500 km in the morning is often greater than the topside F region O^+ temperature.

9. Our observations of the solar cycle variation of the hydrogen abundance above the exobase are similar to that inferred from previous observations and are described well by current exospheric models. The measured H_α intensities, when adjusted for the solar Ly β flux, confirm many earlier studies which show that thermal escape is not the sole mechanism for escape.

Technological improvements in several components of the Fabry-Perot interferometer have resulted in the acquisition of high-quality spectral profiles of a weak airglow emission. Simultaneous observations of H_α with incoherent scatter measurements at various locations on the earth can begin to reveal the morphology of the exosphere in an analagous manner to current studies of the thermosphere. Such an endeavor would begin to reveal the dynamics of the exosphere, as well as the coupling between the dynamics of the thermosphere and exosphere.

APPENDIX

The fine-structure components of the hydrogen Balmer alpha n=3 to n=2 transition are listed in Table 6. Only the $3^2P_{3/2}$–$2^2S_{1/2}$ and $3^2P_{1/2}$–$2^2S_{1/2}$ transitions (numbers 4 and 5 in Table 6) follow excitation of the ground state hydrogen atom by solar Ly β. The orbital and total angular momentum selection rules ($\Delta l = \pm 1$, $\Delta j = 0, \pm 1$) dictate that excitation from the ground state may populate only two of the fine-structure components of the n=3 energy level, $3^2P_{3/2}$ and $3^2P_{1/2}$. A transition from n=3 to n=2 in the Balmer series takes place only to the $2^2S_{1/2}$ level, again because of the Δl selection rule. Thus geocoronal H_α is a two-line emission, separated by 0.0465 Å, in the absence of collisional excitation of the remaining n=3 fine-structure levels.

If collisional excitation does occur, the remaining fine-structure components of the n=3 energy level may be populated and each allowed transition from n=3 to n=2 will be red shifted away from the composite $3^2P_{3/2}$, $3^2P_{1/2}$–$2^2S_{1/2}$ emission, with the exception of transition 3 (Table 6). The composite line center of geocoronal H_α which results from solar Ly β excitation occurs at 6562.7194 Å in dry air under conditions of standard temperature and pressure.

Synthetic two-line emissions have been convolved with a synthetic instrument function and summed in wavelength space to determine the nature of the composite geocoronal emission. Figure 16 shows examples of the resultant line emission for the range of spectral resolutions we have used for observations. It is evident that the two profiles form a composite profile that is indistinguishable from a Gaussian profile, although the summed profile is broader than its two components. Also, the line center of the composite line is shifted from the line center of either of the constituents. The quantity Δv in Table 6 is calculated with respect to the composite line center.

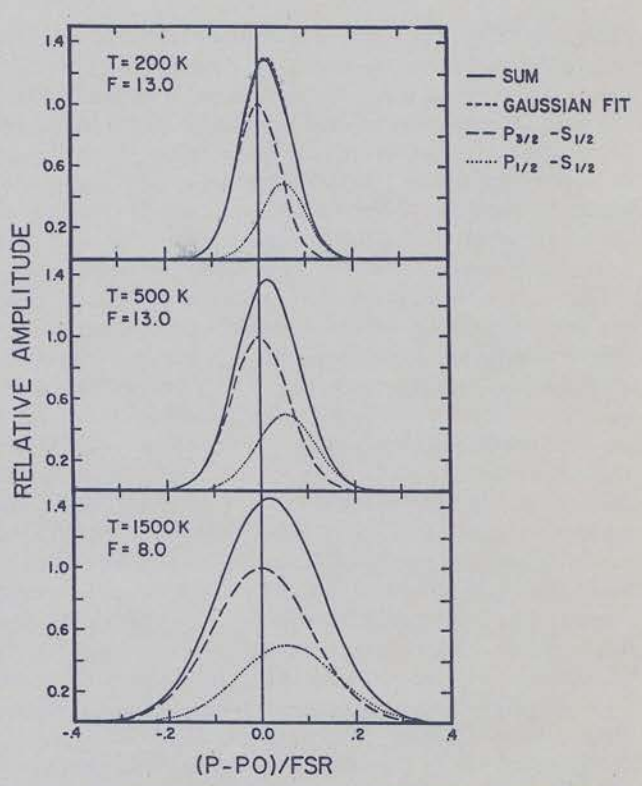

Fig. 16. Synthetic profiles of the two components of geocoronal H_α and their sum. Each summed profile is also fit with a Gaussian function, although this fit is only evident in Figure 16*a*. These profiles encompass the range of spectral resolutions that have been used in our observations. F is the instrumental finesse.

Figure 17 illustrates the temperature error that would be incurred by assuming the geocoronal Hα line is a single-emission line. In fact, Figure 17 contains two curves, one for an instrumental finesse of 13.0, and one for an instrumental finesse

TABLE 6. Balmer Alpha Fine Structure

No.	Transition, n=3–n=2	Relative[a] Intensity	Transition[a] Probability, 10^8 s^{-1}	λ_{Air}[b], Å	Δv[c], km s^{-1}
1	$D_{5/2}$–$P_{3/2}$	1.000	0.643	6562.845	5.746
2	$D_{3/2}$–$P_{3/2}$	0.110	0.107	6562.861	6.455
3	$D_{3/2}$–$P_{1/2}$	0.560	0.536	6562.704	−0.713
4	$P_{3/2}$–$S_{1/2}$	0.230	0.223	6562.704	−0.713
5	$P_{1/2}$–$S_{1/2}$	0.115	0.223	6562.750	1.413
6	$S_{1/2}$–$P_{1/2}$	0.011	0.021	6562.750	1.413
7	$S_{1/2}$–$P_{3/2}$	0.022	0.042	6562.907	8.529

[a] Data from *Condon and Shortley* [1964].
[b] Dry air at 15°C, 76 cm Hg.
[c] Shift from geocoronal line center at 6562.7194 Å.

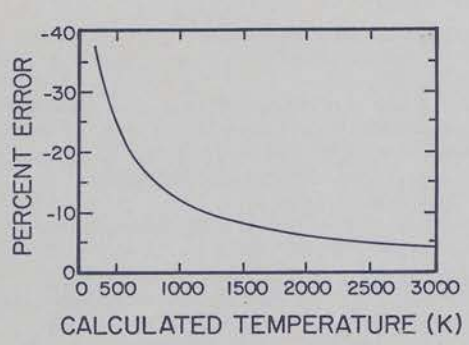

Fig. 17. Percent error in calculated temperature that occurs if the geocoronal H_α emission is treated as a single-line emission. The curve is identical for the range of spectral resolutions used in our observations because the two component emission lines are unresolved.

of 8.0. That these two curves are superimposed merely indicates that the components of the emission line remain entirely unresolved for the range of resolutions that we have employed to measure the geocoronal emission. Because of this, Figure 17 overstates the complexity of adjusting for the composite line broadening. In fact, the width of the composite emission is simply broader by 120 K than the width characteristic of the actual atmospheric temperature. This value is constant for the full range of temperatures and spectral resolutions appropriate for our data. Figure 16 shows that the two line components begin to be slightly resolvable for a finesse of 13.0 and an emission temperature of 200 K, but this temperature is unrealistically cold for exospheric emissions.

Acknowledgements. The authors thank the scientific and maintenance staff at the Arecibo Observatory for their contributions to the success of our experiments. We are grateful for the comprehensive reviews of this paper by the referees and thank J. R. Bertaux for discussions on multiple scattering and for critically reviewing the manuscript. We also thank Geoff Shaughnessy for his assistance with data reduction. This work was performed under National Science Foundation grant ATM-8109257 and ATM-8419730. The Arecibo Observatory is operated by Cornell University under contract with the National Science Foundation.

The Editor thanks the two referees for their assistance in evaluating this paper.

REFERENCES

Atreya, S. K., An investigation into the geocoronal and interplanetary hydrogen Balmer emissions, Ph.D. thesis, 190 pp., Univ. of Mich., Ann Arbor, 1973.

Atreya, S. K., P. B. Hays, and A. F. Nagy, Doppler profile measurements of the geocoronal hydrogen Balmer alpha line, *J. Geophys. Res.*, *80*, 635–638, 1975.

Bailey, G. J., J. F. Vickrey, and W. E. Swartz, The topside ionosphere above Arecibo during summer of sunspot minimum and the influence of interhemispheric flow of thermal protons, *J. Geophys. Res.*, *87*, 7557–7567, 1982.

Bertaux, J. L., Observed variations of the exospheric hydrogen density with the exospheric temperature, *J. Geophys. Res.*, *80*, 639–642, 1975.

Bertaux, J. L., Interpretation of OGO-5 shape measurements of Lyman α emission from terrestrial exospheric hydrogen, *Planet. Space Sci.*, *26*, 431–447, 1978.

Bertaux, J. L., and J. E. Blamont, Interpretation of OGO 5 Lyman alpha measurements in the upper geocorona, *J. Geophys. Res.*, *78*, 80–91, 1973.

Breig, E. L., S. Sanatani, and W. B. Hanson, Thermospheric hydrogen: the long term solar influence, *J. Geophys. Res.*, *90*, 5247–5260, 1985.

Burnside, R. G., J. C. G. Walker, R. A. Behnke, and C. A. Tepley, Plasma dynamics in the nighttime *F* region at Arecibo, *J. Atmos. Terr. Phy.*, *47*, 925–939, 1985.

Chamberlain, J. W., Planetary coronae and atmospheric evaporation, *Planet. Space Sci.*, *11*, 901–960, 1963.

Chamberlain, J. W., Spectral line profiles for a planetary corona, *J. Geophys. Res.*, *81*, 1774–1776, 1976.

Chamberlain, J. W., Charge exchange in a planetary corona: Its effect on the distribution and escape of hydrogen, *J. Geophys. Res.*, *82*, 1–9, 1977.

Chamberlain, J. W., Depletion of satellite atoms in a collisionless exosphere by radiation pressure, *Icarus*, *39*, 286–294, 1979.

Cole, K. D., Theory of some quiet magnetospheric phenomena related to the geomagnetic tail, *Nature*, *211*, 1385–1387, 1966.

Condon, E. U., and G. H. Shortley, *The Theory of Atomic Spectra*, 441 pp., Cambridge, London, 1964.

Donahue, T. M., Hydrogen, in *The Upper Atmosphere and Magnetosphere*, pp. 72–83, Geophysics Study Committee, National Research Council, National Academy of Science, Washington, D.C., 1977.

Emerich, C., and S. Cazes, Local perturbations of the atomic hydrogen density distribution near the exobase, inferred from D2A airglow measurements, *Geophys. Res. Lett.*, *4*, 523–526, 1977.

Emerich, C., S. Cazes, and J. E. Blamont, Exobase hydrogen density temperature from Ly alpha absorption and polarization measurements, 2, Dayside and nightside results during April 1971, *J. Geophys. Res.*, *81*, 6103–6114, 1976.

Fahr, H. J., Reduced hydrogen temperature in the transition region between thermosphere and exosphere, *Ann. Geophys.*, *32*, 277–282, 1976.

Fahr, H. J., and H. U. Nass, Concerning the structure of the transition layer between the terrestrial atmosphere and the exosphere, *Ann. Geophys.*, *34*, 219–230, 1978.

Fahr, H. J., and G. Paul, Exospheric velocity distribution functions and derived gas dynamical properties, *J. Atmos. Terr. Phys.*, *38*, 841–846, 1976.

Fahr, H. J., and B. Shizgal, Modern exospheric theories and their observational relevance, *Rev. Geophys.*, *21*, 75–124, 1983.

Hanson, W. B., and H. C. Carlson, The ionosphere, in *The Upper Atmosphere and Ionosphere*, pp. 84–101, Geophysical Study Committee, National Research Council, National Academy of Science, Washington, D.C., 1977.

Hedin, A. E., A revised thermospheric model based on mass spectrometer and incoherent scatter data, *J. Geophys. Res.*, *88*, 10,170–10,188, 1983.

Hinteregger, H. E., Representations of solar EUV fluxes for aeronomical applications, *Adv. Space Res.*, *1*, 39–52, 1981.

Ho, M. C., and D. R. Moorcraft, Hydrogen density and proton flux in the topside ionosphere over Arecibo, Puerto Rico, from incoherent scatter observations, *Planet. Space Sci.*, *19*, 1441–1455, 1971.

Ho, M. C., and D. R. Moorcraft, Composition and temperatures of the topside ionosphere over Arecibo, *Planet. Space Sci.*, *23*, 315–322, 1975.

Hodges, R. R., Jr., R. P. Rohrbaugh, and B. A. Tinsley, The effect of the charge exchange source on the velocity and 'temperature' distributions and their anisotropies in the earth's exosphere, *J. Geophys. Res.*, *86*, 6917–6925, 1981.

Hunten, D. M., The escape of light gases from planetary atmospheres, *J. Atmos. Sci.*, *30*, 1481–1494, 1973.

Hunten, D. M., Thermal and nonthermal escape mechanisms for terrestrial bodies, *Planet. Space Sci.*, *30*, 773–783, 1982.

Hunten, D. M., and T. M. Donahue, Hydrogen loss from the terrestrial planets, *Ann. Rev. Earth Planet. Sci.*, *4*, 265–292, 1976.

Hunten, D. M., and D. F. Strobel, Production and escape of terrestrial hydrogen, *J. Atmos. Sci.*, *31*, 305–317, 1974.

Jeans, J. H., *The Dynamical Theory of Gases*, 4th ed., Cambridge University Press, New York, 1925.

Kerr, R. B., S. K. Atreya, J. W. Meriwether, Jr., R. G. Burnside, and C. A. Tepley, Simultaneous measurements of the geocoronal Balmer alpha emission and the *F* region oxygen temperature at Arecibo, (abstract) *Eos Trans. AGU*, *65*, 251, 1984.

Liu, S. C., and T. M. Donahue, Mesospheric hydrogen related to exospheric escape mechanisms, *J. Atmos. Sci.*, *31*, 1466–1470, 1974a.

Liu, S. C., and T. M. Donahue, Realistic model of hydrogen constituents in the lower atmosphere and escape flux from the upper atmosphere, *J. Atmos. Sci.*, *31*, 2238–2242, 1974*b*.

Maher, L. J., and B. A. Tinsley, Atomic hydrogen escape rate due to charge exchange with hot plasmaspheric ions, *J. Geophys. Res.*, *82*, 689–695, 1977.

Maher, L. J., and B. A. Tinsley, The diurnal and solar cycle variation of the charge exchange induced hydrogen escape flux, *Planet. Space Sci.*, *26*, 855–861, 1978.

Meier, R. R., Balmer alpha and Lyman beta in the hydrogen geocorona, *J. Geophys. Res.*, *74*, 3561–3574, 1969.

Meriwether, J. W., Jr., S. K. Atreya, T. M. Donahue, and R. G. Burnside, Measurements of the spectral profile of Balmer alpha emission from the hydrogen geocorona, *Geophys. Res. Lett.*, *7*, 961–970, 1980.

Prisco, R. A., and J. W. Chamberlain, Spectral line profiles in a planetary corona: A collisional model, *J. Geophys. Res.*, *83*, 2157–2161, 1978.

Prisco, R. A., and J. W. Chamberlain, Doppler line profiles in a planetary corona: An extended approach, *J. Geophys. Res.*, *84*, 4363–4370, 1979.

Reynolds, R. G., Interstellar Hα emission along the galactic equator, *Astrophys. J.*, *268*, 698–709, 1983.

Reynolds, R. J., F. Scherb, and F. L. Roesler, Observations of diffuse galactic H and [N II] emission, *Astrophys. J.*, *185*, 869–875, 1973.

Reynolds, R. J., F. L. Roesler, and F. Scherb, The intensity distribution of diffuse galactic H_α emission, *Astrophys. J.*, *192*, L53–L56, 1974.

Shih, P., Intensity variations of geocoronal Balmer alpha emission, Ph.D. thesis, 124 pp., Univ. of Wis., Madison, 1983.

Shih, P., F. L. Roesler, and F. Scherb, Intensity variations of geocoronal Balmer alpha emission, 1, Observational results, *J. Geophys. Res.*, *90*, 477–490, 1985.

Shizgal, B., and M. S. Lindenfeld, A simple kinetic theory calculation of terrestrial atomic hydrogen escape fluxes induced by charge exchange collisions, *J. Geophys. Res.*, *87*, 853–858, 1982.

Thomas, G. E., and D. E. Anderson, Jr., Global atomic hydrogen density derived from OGO-6 Lyman alpha measurements, *Planet. Space Sci.*, *24*, 303–312, 1976.

Thomas, G. E., and A. Vidal-Madjar, Latitude variations of exospheric hydrogen and the polar wind, *Planet. Space Sci.*, *26*, 873–882, 1978.

Tinsley, B. A., The diurnal variation of atomic hydrogen, *Planet. Space Sci.*, *21*, 686–691, 1973.

Tinsley, B. A., Effects of charge exchange involving H and H^+ in the upper atmosphere, *Planet. Space Sci.*, *26*, 847–853, 1978.

Tinsley, B. A., R. R. Hodges, Jr., and D. F. Strobel, Diurnal variations of atomic hydrogen: Observations and calculations, *J. Geophys. Res.*, *80*, 626–634, 1975.

Vickrey, J. F., W. E. Swartz, and D. T. Farley, Ion transport in the topside ionosphere at Arecibo, *J. Geophys. Res.*, *84*, 7307–7314, 1979.

Vidal-Madjar, A., The earth hydrogen exobase near a solar minimum, *Geophys. Res. Lett.*, *5*, 29–32, 1978.

Vidal-Madjar, A., and G. E. Thomas, The terrestrial hydrogen problem, *Planet. Space Sci.*, *26*, 863–871, 1978.

Yelle, R. V., and F. L. Roesler, High resolution observations of geocoronal Balmer alpha emissions, (abstract) *Eos Trans. AGU*, *65*, 251, 1984.

Yelle, R.V., and F.L. Roesler, Geocoronal Balmer alpha line profiles and implications for the exosphere, *J. Geophys. Res. 90*, 7568, 1985.

S. K. Atreya and R. B. Kerr, Atmospheric and Oceanic Science Department, College of Engineering, University of Michigan, Space Research Building, Ann Arbor, MI 48109.

R. G. Burnside and C. A. Tepley, Arecibo Observatory, Cornell University, PR 00613.

J. W. Meriweather, Jr., Space Physics Research Laboratory, College of Engineering, University of Michigan, Space Research Building, Ann Arbor, MI 48109.

(Received February 12, 1985;
revised November 13, 1985;
accepted November 20, 1985.)